Journal of Energy Storage 33 (2021) 102067

Contents lists available at ScienceDirect

Journal of Energy Storage

journal homepage: www.elsevier.com/locate/est

On the assessment of specific heat capacity of nanofluids for solar energy applications: Application of Gaussian process regression (GPR) approach

Mehdi Jamei [a], Iman Ahmadianfar [b], Ismail Adewale Olumegbon [c], Masoud Karbasi [d], Amin Asadi [e,f,*]

[a] Faculty of Engineering, Shohadaye Hoveizeh University of Technology, Dasht-e Azadegan, Susangerd, Iran
[b] Department of Civil Engineering, Behbahan Khatam Alanbia University of Technology, Behbahan, Iran
[c] Department of Physical and Chemical Sciences, Elizade University, Ondo State, Nigeria
[d] Water Engineering Department, Faculty of Agriculture, University of Zanjan, Zanjan, Iran
[e] Institute of Research and Development, Duy Tan University, Da Nang 550000, Vietnam
[f] Faculty of Natural Sciences, Duy Tan University, Da Nang 550000, Vietnam

ARTICLE INFO

Keywords:
Specific heat capacity
Solar energy
Nanofluids
Volume fraction
Gaussian process regression

ABSTRACT

To characterize the performance of nanofluids for heat transfer applications in solar systems, an accurate estimation of their specific heat capacity (SHC) is of paramount importance. To this end, having such properties of nanofluids via computational approaches has gained attention as an effective method to eliminate the time-consuming process of experimental investigations. This study focuses on modeling the SHC of different carbon-based and metal oxide-based nanoparticles dispersed in various base fluids. Herein, we propose a novel data-driven dynamic model based on the Gaussian process regression (GPR) technique in comparison with the random forest (RF) approach and generalized regression neural network (GRNN) to predict the SHC of nanofluids. The developed models employ the solid volume fraction (ϕ), temperature (T), mean diameter of nanoparticle (D_p), and SHC of base fluid (C_P^{Base}) as the input parameters. The data has been collected from 10 reliable references. The results showed that the GPR model (R=0.99974, RMSE=0.01506 J/K.g) shows superior performance than the results of the RF (R=0.99761, RMSE=0.04598 J/K.g) and GRNN (R=0.99563, RMSE=0.06085 J/K.g). The results proved that the developed model would accurately estimate the SHC of the studied nanofluids. In addition, the sensitivity analysis of the dependence of input variables on the SHC of nanofluids revealed that the mean diameter of nanoparticles and the SHC of base fluid are the major critical factors in the determination of SHC of nanofluids.

1. Introduction

Nanofluids are a product of the homogenous suspension of nanoparticles in conventional fluids. The resulting fluid mixture possesses enhanced thermo-physical properties such as specific heat capacity (SHC), density, viscosity, thermal conductivity, and so forth [1,2]. The small size and large surface to volume ratio of nanoparticles can be the effective factors to enhance the thermal conductivity of nanofluids. In addition, they have the capability to move easily in flow-channels with less particle momentum and have a higher heat transfer rate than conventional fluids [3,4].

In recent years, the number of published research on nanofluids has increased enormously. The capability of nanofluids in enhancing the heat transfer makes them the desired material of choice for energy-saving applications [5,6]. Thus, they have the capability to reduce energy costs and to increase the market size of nanofluid based technologies exponentially to over 2 billion dollars annually [7]. For example, the use of nanofluids in electricity generation has improved chiller efficiency by 1 %, thereby saving an estimated 320 billion *kWh* of electricity equivalent to 5.5 million barrels of oil annually [7]. Certainly, nanofluids are significant materials for effective energy management capable of reducing global warming and energy crisis [6]. Moreover, they continuously receive massive attention from solar energy researchers owing to its contribution in the areas of solar thermoelectric devices [8], solar water heaters [9,10], solar collectors [11,12],

Abbreviations: CNT, carbon nanotube; EG, ethylene glycol; MWCNT, multi-walled carbon nanotube RD, relative deviation; SHC, specific heat capacity; W, water.

* Corresponding author.
E-mail address: aminasadi@duytan.edu.vn (A. Asadi).

https://doi.org/10.1016/j.est.2020.102067
Received 29 August 2020; Received in revised form 12 October 2020; Accepted 29 October 2020
Available online 12 November 2020

Nomenclature

C_P^{Base}	specific heat capacity of base fluid (J/K.g)
C_P^{nf}	specific heat capacity of nanofluid (J/K.g)
C_P^{np}	specific heat capacity of nanoparticle (J/K.g)
E_r	relative deviation
D_p	particle diameter, nm
I_w	index of agreement
m	mass (g)
MAPE	mean absolute percentage error
P_c	Pearson correlation coefficient
R	correlation coefficient
RAE	relative absolute error
RMSE	root mean square error (J/K.g)
SI	scatter index
T	temperature, (K)

Greek

ϕ	nanoparticle volume fraction (-)
ρ_{nf}	bulk fluid density, g/cm3
ρ_{np}	density of the nanoparticles, g/cm3
ρ_{bf}	density of the base fluid, g/cm3
κ	thermal diffusivity (m^2/s)

Subscripts

bf	base fluid
i	nanoparticle ID
nf	nanofluid
np	nanoparticle
ω	nanoparticle mass fraction

solar-geothermal combined cooling, heating, and power systems [13–15], and so forth. Unlike conventional heat transfer fluids, nanofluids are better absorbers of radiation over the ultra-violet and visible light region of the solar radiation spectrum. This feature enables them as a suitable alternative for solar energy applications; they improved solar radiation absorption in the direct absorption solar collectors (DASC) system [16–18]. Nanoparticles are mainly composed of metals, non-metals, metal oxide, and other compounds [19–22]. The choice of nanoparticle/base fluid combination for the production of nanofluid is governed by some crucial factors like chemical stability, toxicity, thermal properties, cost, availability, and compatibility [23]. Nanofluids have been successfully deployed in many technological applications as they are generally preferred because of their relative cheapness [24], ease of production, chemical stability, and poses a lesser particle settling problems during production [25,26]. Nanofluids are utilized for heat transfer purposes in solar thermal systems [27–29] and have been prominently applied in solar collectors because of its ability to enhance the solar collector's optical properties. Tubular solar collectors have employed Al_2O_3/water, ZnO/water, and MgO/water as nanofluids [17], evacuated tube solar collectors use SWCNT/water [30] and MWCNT/water [31], DASC uses Sand/PG-water [32] and ZnO/PG-water nanofluid [33], flat plate solar collector uses Cu/water [34], and Cu-synthesized/EG [35], and CuO/water nanofluid [7], and many more.

The specific heat capacity of nanofluids is a measure of the capacity of the nanofluid to retain heat. This makes it an essential thermal property that defines the nanofluid. Moreover, it helps in quantifying the thermal characteristics of any system by using the thermal diffusivity [6, 36–41], as evident in Eqs. (1) and (2). It occupies a significant position in the design of heat management systems and heat transfer applications. It helps in quantifying effective heat energy management strategies that will optimize energy conservation and minimize energy loss in a system [42]. Hence, its accurate determination becomes expedient. The relationship between the SHC and thermal conductivity can be expressed as follows:

$$\alpha = \frac{\kappa}{\rho C_P^{nf}} \tag{1}$$

whereα, κ, ρ, $C_p$represent thermal diffusivity, thermal conductivity, density, and SHC, respectively.

The most popular theoretical SHC prediction models are model (I) and model (II), which are based on the concepts of mixing theory for ideal gas mixtures and the first law of thermodynamics. For this reason, these models are known as mixing model (I) and thermal equilibrium model (II) [43–46]. The mixing model comprised the relationship between the SHC of nanofluid, nanoparticles, and base fluid as follows [43, 47]:

$$C_{PI} = \phi\, C_P^{np} + (1-\phi) C_P^{Base} \tag{2}$$

where ϕ, C_P^{nf}, C_P^{np}, and C_P^{Base} represent the nanoparticle volume fraction, SHC of nanofluid, SHC of nanoparticles, and SHC of the base fluid, respectively. The nanoparticle volume fraction can be converted to the corresponding mass fraction using the following equation:

$$\phi = \frac{w}{w + (\rho_{np}/\rho_{bf})(1-w)} \tag{3}$$

For better explanation of the experiment conditions, model (I), which is based on the thermal equilibrium between nanoparticles and the base fluid, can also be expressed in terms of densities and volume fraction in the form of model (II) as follows [43–45,48].

$$C_{PII} = \frac{\varphi\rho_{np}C_P^{np} + (1-\varphi)\rho_{bf}C_P^{Base}}{\varphi C_P^{np} + (1-\varphi)\rho_{bf}},\ \rho_{nf} = (1-\phi)\rho_{bf} + \phi\rho_{np} \tag{4}$$

where $\rho_{nf}, \rho_{np}, \rho_{bf}$ represent the nanofluid density, nanoparticle density, and base fluid density, respectively.

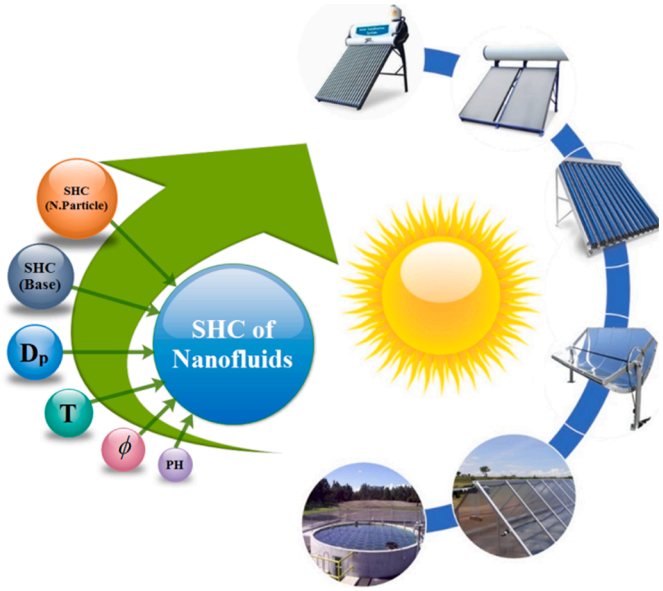

Fig. 1. The schematic view of nanofluids application in the solar energy systems and influence factor in Specific heat capacity of nanofluids.

Table 1
Experimental investigation of nanofluids' SHC.

Nanofluids	Base fluid	Studied factors	Equipment	Reference
Al_2O_3	water-Ethylene glycol	Nanoparticle volume fraction, temperature	Micro DSC II micro-calorimeter	Barbes et al. [41]
Al_2O_3, ZnO, SnO	Ethylene glycol water, water	Nanoparticle volume fraction, temperature	Unspecified	Vajjha et al. [55]
Al2O3	water	Nanoparticle volume fraction	Differential scanning calorimeter (DSC)	Zhou et al. [56]
Al_2O_3	water-Ethylene glycol	Nanoparticle volume fraction, temperature	Differential scanning calorimeter (DSC)	Elias et al. [57]
CuO	water-Ethylene glycol	Nanoparticle volume fraction, temperature	Micro DSC II micro-calorimeter	Barbes et al. [49]
Cu	Ethylene glycol	pH, temperature	Modulated temperature Differential scanning calorimeter (MTDSC)	Robertis et al. [58]
Metal, metal oxides	poly-a olefin, mineral oil, ethylene glycol, the mixture of water and ethylene glycol, and calcium nitrate tetrahydrate	Nanoparticle mass fraction, the heat capacity of the base fluid	Differential scanning calorimeter (DSC)	Starace et al. [59]
MWCNT	water-Ethylene glycol	Nanoparticle volume fraction, temperature	Differential scanning calorimeter (DSC)	Kumaresan et al. [60]
MWCNT	distilled water	Nanoparticle volume fraction, temperature	Differential scanning calorimeter (DSC)	Sabiha et al. [61]
TiO_2, Al_2O_3, Al	DI-water, Ethylene glycol, Engine-oil	Nanoparticle volume fraction and type, base fluid type	Double-hot wire technique	Murshed et al. [62]
TiO_2, Al_2O_3	Water, ethylene glycol	Nanoparticle concentration, temperature	Differential scanning calorimeter (DSC)	Nieh et al. [63]
β-CD MWCNT	Ethylene glycol	Nanoparticle concentration, Nanoparticle volume fraction, temperature	Simultaneous thermal analyzer	Li et al. [64]

Pak and Cho, as a pioneer, conducted the experimental investigation on the SHC of Al_2O_3/Water and TiO_2/Water estimation [43]. Over the last decades, several research efforts have experimented with a variety of nanofluids and proved that the SHC of nanofluids is dependent upon a number of physical and chemical properties such as the nanoparticle size (D_p), volume fraction (ϕ), PH, SHC of base fluid (C_P^{Base}), SHC of nanoparticle (C_P^{np}), temperature, and so forth [41,49,50]. Fig. 1 depicted the schematic view of the effective factors that govern the SHC of nanofluids estimation and nanofluids application in solar energy applications. Besides, a summary of the experimental investigation of nanofluids' SHC is presented in Table 1.

Consequent to the myriad of factors affecting the SHC of nanofluids, their experimental investigation can be rigorous, taking into account the number or combination of factors to be considered, hence affecting the timely determination of the SHC for heat transfer applications [51]. Moreover, other difficulties, such as the high cost of nanofluids and the sensitivity of synthesis and measurement, poses setbacks to the timely measurements of the SHC [52]. In other words, to avoid performing experimental bottlenecks, especially in the face of limited resources, experimental-based models have proven to be a reliable route. The two main models that have successfully predicted the SHC of nanofluids are the mixing rule model [47] and the thermal equilibrium model [48], generally referred to as model (I) and model (II), respectively. Previous studies have simultaneously employed models (I) and (II) in the determination of the SHC for nanofluids involving different nanoparticles-base fluids combinations, such as Al_2O_3 [53], MgO, ZnO, and SrO_2 dispersed in ethylene glycol (EG)-water [24]. In most of these studies, model (II) resulted in a highly accurate estimation with experimental data as compared with the model (I). However, model (II) gave poor results for some nanofluids [51,52,54].

Inaccuracies associated with the numerical models in the estimation of the SHC is caused by the underlying assumptions between model inputs and target variable coupled with their inability to account for the anomalous nature of nanofluids. As a result, machine learning (ML) techniques are employed because of their robust predictive accuracy. So far, ML models have been developed to predict thermal conductivity [4,65–71], viscosity [67,72–75], and SHC [76–78] using artificial intelligence (AI) models: Artificial Neural Network (ANN) [74,79,80] and Support Vector Regression (SVR) [78,81]. In the case of machine learning studies, the employed algorithms extrapolate data using the nanofluids physico-chemical properties as model inputs and the thermophysical properties as the target variable such that it learns the pattern in the data and establish a relationship which can be explored for future determination of the thermophysical property of choice [82,83]. Alade et al. [77] made the first attempt to estimate the SHC of nanofluids by using the ML model. In their research, support vector regression was developed by a genetic algorithm (GA) to estimate the SHC of Al_2O_3/-water nanofluids [77]. Other machine learning studies deployed in the prediction of SHC of nanofluids are given in Table II. ML models have been deployed to estimate the SHC of metal oxide-based nanofluids. Such studies include the application of SVR techniques for predicting the SHC of CuO-based nanofluids [84,85] and Al_2O_3-based nanofluids [50,52].

In this study, the Gaussian process regression (GPR) technique is used in comparison with the random forest (RF) approach and generalized regression neural network (GRNN) to predict the SHC of nanofluids. These machine learning techniques have been used to develop models capable of estimating nanofluids parameters. The GPR gave a successful estimation of the thermal conductivity of Al_2O_3/H_2O [86,87], CuO/H_2O [86,87], and Battery calendar aging prediction [88,89]. Just recently, the RF approach has been applied to model the viscosity of metal oxide-based nanofluids, such as SiO_2, TiO_2, ZnO, MgO, and so forth [90]. Additionally, GRNN was used to estimate the pool boiling heat transfer coefficient of TiO_2/water [91].

Based on the presented literature above, the lack of having accurate and reliable research on SHC of a wide variety of nanofluids, including metal oxides and carbon dispersed in various base fluids using AI-based methodologies of GPR, RF, and GRNN, is greatly felt. Thus, in this study, it is tried to fill this gap in the available literature. The results of the proposed GPR approach were compared to the RF, GRNN, and existing correlations. Moreover, the authors' survey on the available literature showed that these three ML approaches had not been applied yet to develop a computational model to estimate the SHC of nanofluids. The developed models were validated using several performance metrics, efficient graphical devices, and expert error analysis. The general framework of the intelligent system for the prediction of SHC of nanofluids is depicted in Fig. 2.

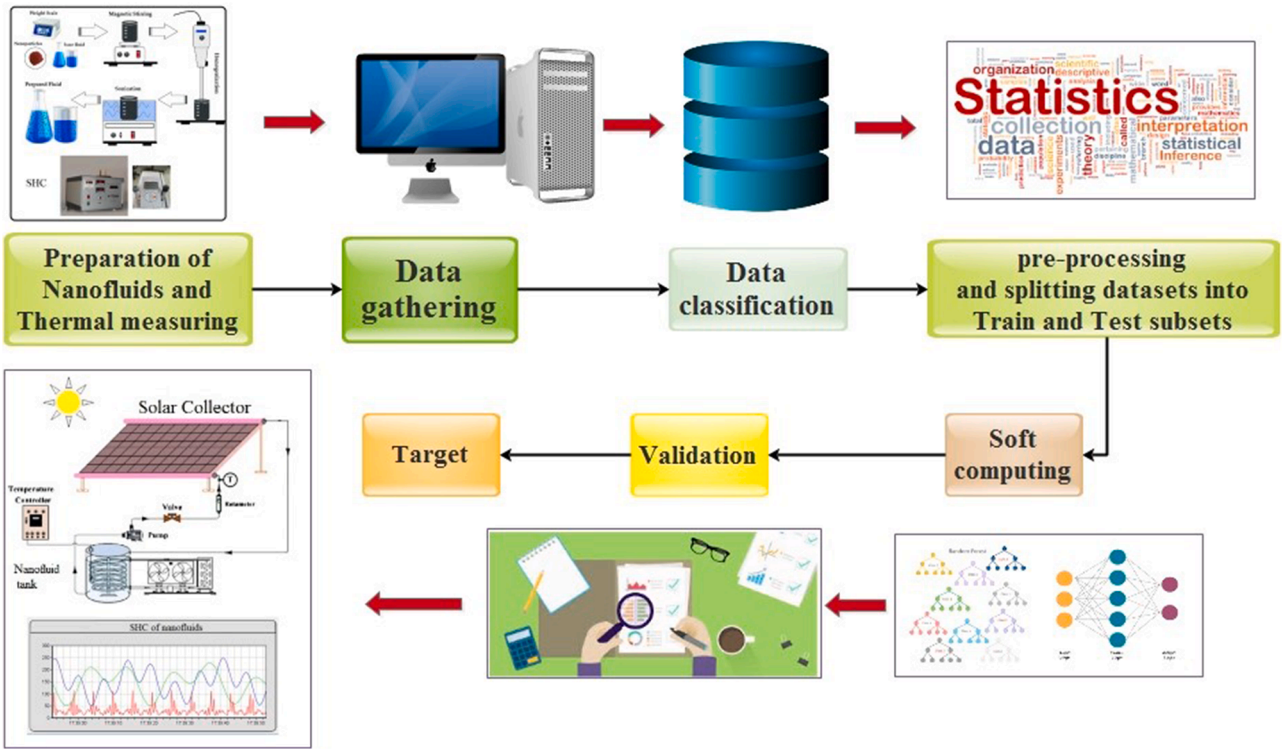

Fig. 2. The general framework of the SHC of nanofluids prediction using developed data-driven models.

2. Methodology

2.1. Gaussian process regression (GPR)

The Gaussian process (GP) is a set of random variables in which a limited number of them are integrated with Gaussian distributions [92]. The GP is fully characterized by its covariance and mean functions. This process is a natural generalization of Gaussian distribution. In this process, mean and covariance are, respectively, a vector and a matrix. Gaussian process regression (GPR) models are based on the assumption that previous observations must carry information about each other. Unlike the Gaussian distribution, the Gaussian process is over functions. As a result, Gaussian process models do not require any validation process to generalize them. Due to prior knowledge of functional dependency and data, Gaussian process regression models are able to understand the predictive distribution corresponding to the test input [93].

Consider the S dataset with n observations. Where $= \{(x_i, y_i)|i = 1, \ldots, n\}$ x_i is the input vector with D dimension and y_i is the target vector. This set consists of two components, input and output, as sample points. In order to facilitate, the inputs of the set are collected in the $X = [x_1, x_2, \ldots, x_n]$ matrix, and the outputs are also aggregated in the $Y = [y_1, y_2, \ldots, y_n]$ matrix.

The task of regression is to create a new input x^* to achieve the predicted distribution for the corresponding values of the observational data y^* based on the S dataset. The Gaussian process $f(x)$ is defined by its mean $m(x)$ function:

$$m(x) = E(f(x)) \tag{5}$$

And the following equation describes covariance $k(x, x')$ functions:

$$k(x, x') = E(f(x) - m(x))(f(x') - m(x')) \tag{6}$$

The Gaussian process is expressed as follows:

$$f(x) \sim GP(m(x), k(x, x')) \tag{7}$$

For simplicity, the mean function value is usually set to zero. In the Gaussian process, the relationship between the target and the input vector is as follows:

$$y_i = f(x_i) + \varepsilon \tag{8}$$

where ε is the value of Gaussian distribution noise with σ^2 variance and zero mean:

$$\varepsilon \sim N(0, \sigma^2) \tag{9}$$

In addition, it is assumed that $f = [f(x_1), \ldots, f(x_n)]^T$ has a behavior based on the Gaussian process, $p(f|X) = N(0, K)$ where K is the covariance matrix with $k_{i,j} = k(x_i, x_j)$ elements.

$$K(x, x) = \begin{bmatrix} K(x_1, x_1) & K(x_1, x_2) & \ldots & K(x_1, x_n) \\ K(x_2, x_1) & K(x_2, x_2) & \ldots & K(x_2, x_n) \\ \vdots & \vdots & \ddots & \vdots \\ K(x_n, x_1) & K(x_n, x_2) & \ldots & K(x_n, x_n) \end{bmatrix} \tag{10}$$

By using GPR, one can compute f^* at test points X^*.

The distribution of y conditioned on the values of f is given as the following equations:

$$P(y|f, X) = N(f, \sigma_n^2 I) \tag{11}$$

where I represents the unit n × n matrix. The marginal distribution of y can be calculated by using the property of Gaussian distribution:

$$P(y|X) = \int p(y|f, X)p(f|X)df = N(0, K + \sigma_n^2 I) \tag{12}$$

The joint distribution of the function values and the observed target values are as follows:

$$\begin{bmatrix} y \\ f_* \end{bmatrix} \sim N\left(\begin{bmatrix} K(X, X) + \sigma^2 I & K(X, X_*) \\ K(X_*, X) & K(X_*, X_*) \end{bmatrix} \right) \tag{13}$$

where $K(X_*, X_*)$ represents the self-covariance matrix of test points (X_*) and $K(X, X_*)$ represents the $n \times 1$ covariance matrix of test points X_* and all the input points X.

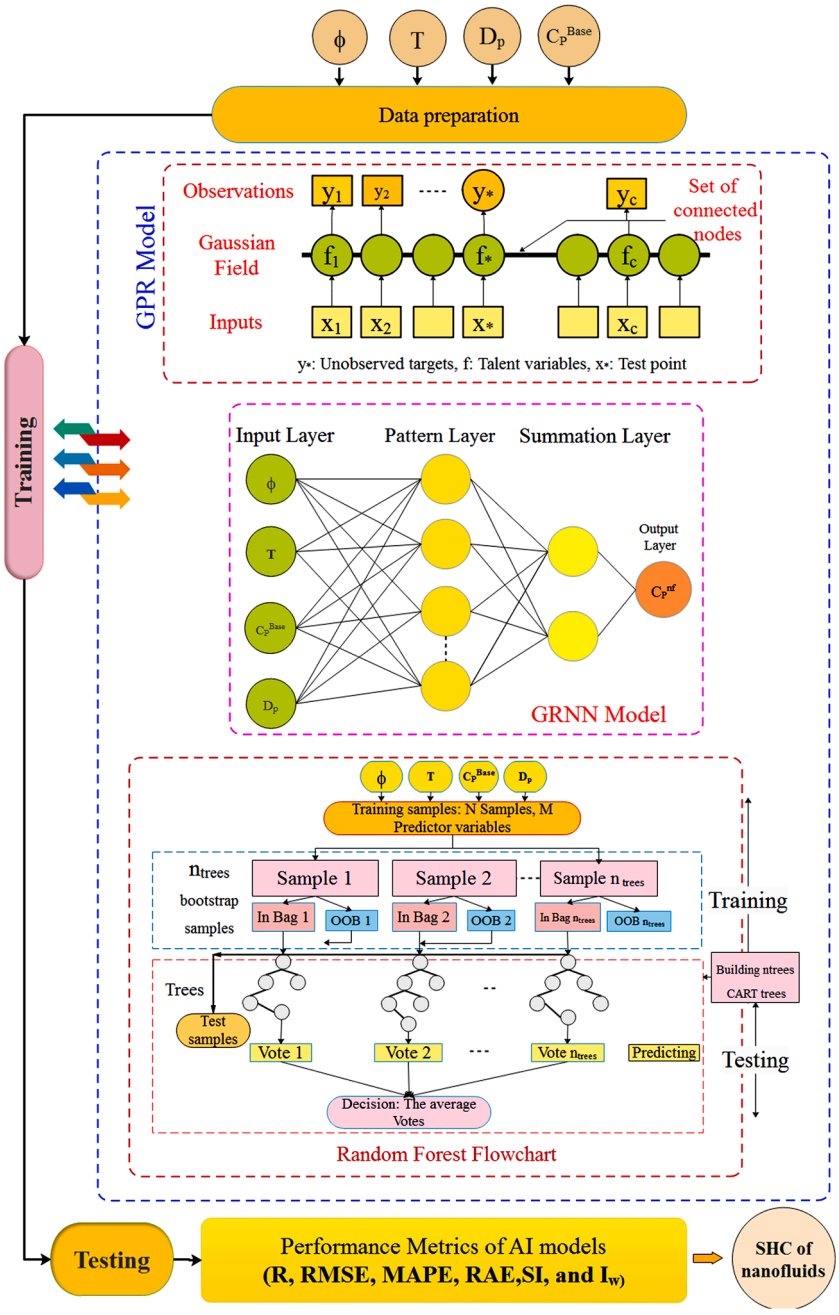

Fig. 3. A. schematic block diagram of the AI-based models for SHC of nanofluids prediction.

When the training process ends, using Bayesian theory, the nearest output values corresponding to X_* can be estimated based on the training set. The probability distribution is updated using the observed data and Bayesian theory. From (3), using the standard rules for conditioning Gaussians, the predictive distribution is obtained as follows:

$$P(f_*|X,y,X_*) \sim N\left(\overline{f_*}, cov(f_*)\right) \tag{14}$$

The output estimates are made by the measure of uncertainty (variance) and expected prediction (mean) of f_* (predictive distribution of the function values).

$$\overline{f_*} = K(X_*,X)\left[K(X,X)+\sigma^2 I\right]^{-1} y \tag{15}$$

$$cov(f_*) = K(X_*,X_*) - K(X_*,X)\left[K(X,X)+\sigma^2 I\right]^{-1} K(X,X_*) \tag{16}$$

The main component of a Gaussian process regression is the covariance or kernel function. The covariance function describes the similarity among the observed data [94]. The following covariance function was used in this research:

Rational Quadratic Kernel

$$k(x_i, x_j|\theta) = \sigma_f^2\left(1+\frac{r^2}{2\alpha\sigma_l^2}\right)^{-\alpha} \tag{17}$$

Matern 3/2

$$k(x_i, x_j|\theta) = \sigma_f^2\left(1+\frac{\sqrt{3}\,r}{\sigma_l}\right)\exp\left[-\frac{\sqrt{3}\,r}{\sigma_l}\right] \tag{18}$$

Matern 5/2

$$k(x_i, x_j|\theta) = \sigma_f^2\left(1+\frac{\sqrt{5}\,r}{\sigma_l}+\frac{5r^2}{3\sigma_l^2}\right)\exp\left[-\frac{\sqrt{5}\,r}{\sigma_l}\right] \quad (19)$$

Squared Exponential Kernel

$$k(x_i, x_j|\theta) = \sigma_f^2\exp\left[-\frac{1}{2}\frac{(x_i-x_j)^T(x_i-x_j)}{\sigma_l^2}\right] \quad (20)$$

Exponential Kernel

$$k(x_i, x_j|\theta) = \sigma_f^2\exp\left[-\frac{r}{\sigma_l}\right] \quad (21)$$

where σ_f is the signal standard deviation, σ_l is the characteristic length scale, and $r = \sqrt{(x_i-x_j)^T(x_i-x_j)}$ is the Euclidean distance between x_i and x_j. Using gradient-based algorithms, the hyperparameters of the covariance function θ (σ_l , σ_f) can be estimated.

2.2. General regression neural network (GRNN)

GRNN is a variant of the RBF neural network. In classification, these networks fall into the category of probabilistic neural networks. Probabilistic networks are able to converge rapidly towards the function with a limited number of training samples, which is an advantage over feed-forward neural networks. Specht [95] proposed a method for formulating a weighted neighborhood approach in the form of neural networks. The GRNN neural networks are often used for function approximation, which includes a radial basis layer and a special linear layer. Each GRNN network has four layers [96] (Fig. 3).

Input layer: In this layer, there is a neuron for each predictor variable. The input neurons are normalized and then feed the values to each of the neurons in the pattern layer.

Pattern layer: This layer has a neuron for each instance in the training data set. Neuron stores predictive values for the target value sample. The pattern P_i is obtained using the Gaussian function as follows:

$$Pi = \exp\left(\frac{(X-X_i)^T(X-X_i)}{2\sigma^2}\right) \quad (22)$$

where σ is the spread parameter (smoothing parameter), X_i is the input vector of n variables.

Summation layer: This layer has two neurons. At this layer, simple summation and the weighted sum of the pattern outputs is determined by:

$$S_s = \sum_{i=1}^{n} P_i \quad (23)$$

$$S_w = \sum_{i=1}^{n} P_i W_i \quad (24)$$

where W_i is the activation weight for the pattern layer i^{th} neuron.

Output Layer: In the output layer, the predicted value is calculated using the following equation:

$$\hat{y} = S_w/S_s \quad (25)$$

2.3. Random forest model

The Random forest model is an efficient learning algorithm using an ensemble of decision trees that can be used for regression or classification [97]. Generally, a combination of decision trees is generated using the random bootstrap samples of the inputs [97]. The main advantages of this approach over the individual regression trees are its reduced probability of overfitting and higher accuracy [97,98]. The RF model needs the number of trees grown (n_{tree}) and feature predictor variables m_{try}. These two parameters are used to control the algorithm behavior [99]. In order to create an RF model, the following steps should be taken (see Fig. 3):

Step 1. Set a value for n_{tree} in the forest

Step 2. Pick a bootstrap sample with size n_{tree} from the input or training dataset to each tree

Step 3. Sample m_{try} from a training dataset with p randomly-selected predictors for the split point in each node.

Step 4. Separate the split-point and the best variable among predictors, and divide each node into two sub-nodes.

Step 5. Calculate the new data by taking the average of the predicted values of each individual tree in the forest.

To generate a forest, the RF creates many random binary trees, and then a bootstrap sample is used to grow trees using the classification and regression trees (CART) method using the random variables chosen at each node [90,100]. Subsequently, the training dataset that is not used in a bootstrap sample is used to calculate the 'out of bag' (OOB) method. OOB is an error rate to determine the prediction error that also evaluates the RF method accuracy and also adjusts the method parameters, e.g., m_{try} [101]. As expected, in order to minimize the OOB error, the values of m_{tree} and m_{try} should be optimized [90,102]. This model is capable of handling high-dimensional databases where many predictors are involved and bothn_{tree}, m_{try} should be adjusted appropriately to avoid overfitting of the RF predictions. One of the challenges of the RF methods is how to determine the optimal number of trees, which is optimal when the OOB error rate is stabilized [103]. An internal optimization function using the decrease in accuracy and mean decrease in node impurity is used to determine the optimal number of predictors m_{try} [100]. In order to implement the RF model, a Matlab's MEX function of Andy Liaw et al.'s C code (used in R package random Forest) is used where the default values of $n_{tree} = 500$ and $m_{try} = Floor(\sqrt{M})$ are suggested, respectively [104]. M is the number of independent predictors or features. To evaluate the predicted relative viscosity of the RF model and assess the variable importance, the mean square error (MSE) of the OOB error rate is determined for each decision tree as follows [97,104]:

$$MSE_{OOB} = \frac{\sum_{i=1}^{n_{tree}}\left(C_{p,i} - C_{pi}^{OOB}\right)^2}{n_{tree}} \quad (26)$$

where C_{pi}^{OOB}represents the mean predicted SHC and $C_{p,i}$ represents the experimental data points. A schematic block diagram of the implemented data-driven approaches for the estimation of the SHC of nanofluids is illustrated in Fig. 3.

3. Performance assessment

To quantify the validation of AI models under consideration, six performance indicators comprised the Correlation Coefficient (R), Root Mean Squared Error (RMSE), Mean Absolute Percentage Error (MAPE), Relative Absolute Error (RAE), Scatter Index (SI), and Willmott's Index of agreement (IW) [105] were used. For a reliable judgment about the accuracy of forecasting in models, if the MAPE value is less than 10%, then the model has the best performance; for 11 ≤ MAPE ≤20, the model has good predictive performance; and for 21≤ MAPE ≤50, the model predicting is reasonable [106].

$$R = \frac{\sum_{i=1}^{N}\left(C_P^{nf}c,i - \overline{C_{P\,c}^{nf}}\right).\left(C_P^{nf}o,i - \overline{C_{P\,o}^{nf}}\right)}{\sqrt{\sum_{i=1}^{N}\left(C_P^{nf}c,i - \overline{C_{P\,c}^{nf}}\right)^2\sum_{i}^{N}\left(C_P^{nf}o,i - \overline{C_{P\,o}^{nf}}\right)^2}} \quad (27)$$

Table 2
Highlight of published works on the use of machine learning methods in predicting the SHC of nanofluids.

Nanofluids	Model inputs	ML methods	Reference
AlN/EG, Si3N4/EG, TiN/EG	Nanoparticles size, Nanoparticles molar mass, Nanoparticles mass fraction, temperature	Bayesian optimized-SVR	Alade et al. [76]
Al_2O_3/molten salt, SiO_2/molten salt, TiO_2/molten salt	Nanoparticles weight fraction, temperature	ANN	Hassan et al. [52]
Al_2O_3/Water	Nanoparticles volume fraction, SHC of nanoparticles	Hybrid genetic algorithm-SVR	Alade et al. [77]
CuO/water	Nanoparticles volume fraction, fluid temperature	SVR and ANN	Alade et al. [84]
CuO/EG, Al_2O_3/EG	SHC of the base fluid, SHC of nanoparticles, the temperature of the base fluid, Nanoparticles volume fraction	Bayesian optimized-SVR	Alade et al. [50]

$$RMSE = \left(\frac{1}{N}\sum_{i=1}^{N}\left(C_P^{nf}o,i - C_P^{nf}c,i\right)^2\right)^{0.5} \quad (28)$$

$$MAPE = \left(\frac{100}{N}\right)\sum_{i=1}^{N}\left|\frac{C_P^{nf}o,i - C_P^{nf}c,i}{C_P^{nf}o,i}\right| \quad (29)$$

$$RAE = \frac{\sum_{i=1}^{N}\left|C_P^{nf}c,i - C_P^{nf}o,i\right|}{\sum_{i=1}^{N}\left|C_P^{nf}o,i - \overline{C_P^{nf}}_o\right|} \quad (30)$$

$$SI = RMSE \Big/ \overline{C_P^{nf}}_o \quad (31)$$

$$I_w = 1 - \frac{\sum_i^N\left(C_P^{nf}o,i - C_P^{nf}c,i\right)^2}{\sum_{i=1}^{N}\left(\left|\left(C_P^{nf}o,i - \overline{C_P^{nf}}_o\right)\right| + \left|\left(C_P^{nf}o,i - \overline{C_P^{nf}}_o\right)\right|\right)^2}, \quad 0 < I_w \le 1 \quad (32)$$

where N is the number of data points, $C_{P\,c,i}^{nf}$ and $C_{P\,o,i}^{nf}$ are the i[th] predicted and measured specific heat capacity of nanofluids, respectively. On the other hand, $\overline{C_P^{nf}}_c$ and $\overline{C_P^{nf}}_o$ are described as the mean value of predicted and measured specific heat capacity of nanofluids, respectively. Furthermore, in order to compare the similarity patterns in polar space between predicted and measured values of C_P^{nf}, the Taylor diagram presents the simultaneous consideration of three statistical measures: R, standard deviation $SDev_i^2 = \frac{1}{N}\sum_{i=1}^{N}\left(C_P^{nf}i - \overline{C_P^{nf}}_i\right)^2$, and centered Root Mean Square Error ($cRMSE^2 = SDev_o{}^2 + SDev_p{}^2 - 2RSDev_o.SDev_p$) [107]. The R is represented by the azimuthal position; the standard deviation is computed by using the radial distance from the origin and ultimately *cRMSE* is introduced by the concentric circular arcs [107].

4. Data collecting and pre-processing

The selection of influential variables (or independent parameters) is an essential part of developing an AI-based model, which should be performed meticulously [108,109]. According to the previous experimental studies on the assessment of SHC of nanofluids in Table 2, various influential parameters have been used as input of the AI-based model.

Among all the input parameters, four independent variables as the solid volume fraction (ϕ), temperature (T), mean diameter of nanoparticle (D_p), and the SHC of base fluid (C_P^{Base}) were considered to develop the predictive models for precise estimating the SHC of nanofluids. The functional relation between predictive independent variables and target (C_P^{nf}) is expressed as:

$$C_P^{nf} = f\left(\phi, T, C_P^{Base}, D_p\right) \quad (33)$$

$$\phi = \frac{\left(\frac{m}{\rho}\right)_{np}}{\left(\frac{m}{\rho}\right)_{np} + \left(\frac{m}{\rho}\right)_{bf}} \quad (34)$$

where ρ and m are the density and mass of the nanoparticle, respectively.

The predictive AI-based models are developed using a total of 1051 reliable experimental data points that are collected from 10 references [43,55,57,61,110–114]. The comprehensive characteristics of implemented data points are tabulated in Table 3. In this study, the data set

Table 3
Details of the employed experimental data points for designing the predictive SHC models.

References	Number of data	Nanoparticle	Base fluid
[43,57,110]	425	Al_2O_3	Water, EG, (50:50)% EG/Water
[49]	189	CuO	Water, EG
[114]	55	CD-CNTs	EG
[111, 113]	45	MWCNT (CNT)	(30:70)% EG/DI.Water, Transformer Oil
[55]	135	SiO_2	(60:40)% EG/Water
[61]	25	SWCNT	Water
[43,112]	60	TiO_2	Water, $BaCl_2$–H_2O
[55]	115	ZnO	(60:40)% EG/Water

Table 4
The descriptive statistics of predictive variables and targets.

	φ(%)	T(K)	C_P^{Base}(J/K.g)	D_P(nm)	C_P^{nf}(J/K.g)
Minimum	0.005	273.200	2.037	1.500	1.201
Maximum	10.000	392.600	4.196	77.000	4.288
Range	9.995	119.500	2.159	75.500	3.087
Mean	3.554	326.000	3.373	36.510	3.109
Std. deviation	3.152	19.580	0.601	18.570	0.634
Skewness	0.683	0.223	-0.246	0.661	-0.081
Kurtosis	-0.820	0.118	-0.936	0.185	-0.915

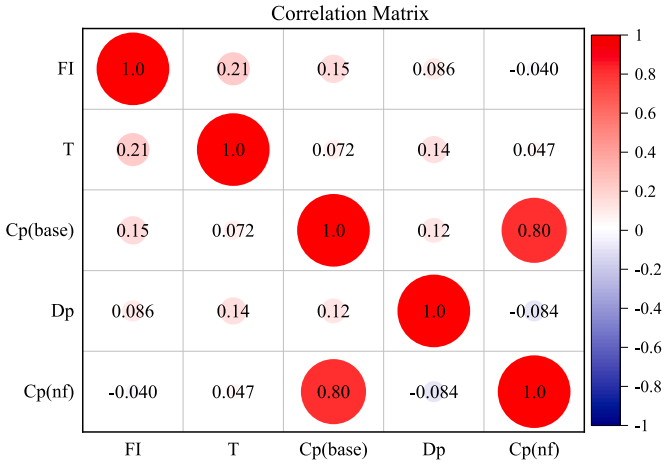

Fig. 4. The correlation matrix between the input and output variables.

Table 5
The correlation and RMSE values for assessment of the optimum covariance function implemented in the GPR model.

	Covariance function					
	Statistical criteria	Matern32	Matern52	Squared exponential	Rational quadratic	Ard exponential
Training	R	0.992539	0.993094	0.993066	0.993066	0.999998
	RMSE	0.076695	0.07376	0.073879	0.073879	0.001153
Testing	R	0.981808	0.985407	0.987739	0.987739	0.99974
	RMSE	0.12543	0.1129	0.104049	0.104049	0.015064

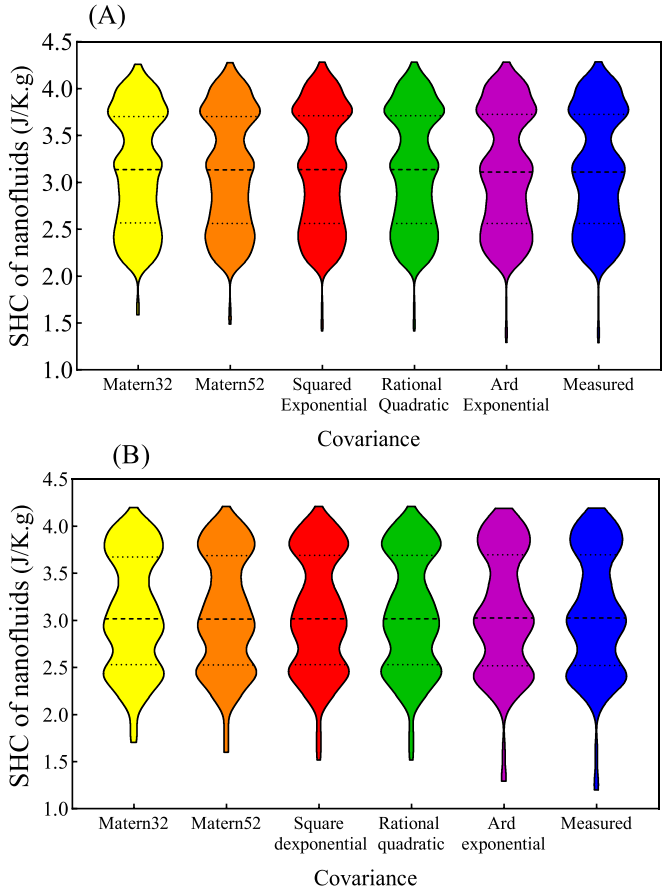

Fig. 5. The violin plot of the implemented covariance function in the GPR model for (A) training and (B) testing stages.

was randomly divided into two sections: 75% (788 data points) and 25% (263 data points) of data points, which were used to perform training and testing stages, respectively. The descriptive statistics of datasets are reported in Table 4. A survey on statistical features of data sets demonstrated that volume fraction and mean diameter of nanoparticle have a large skewness coefficient, indicating a significant difference between the mean and median values of these predictive variables. Based on existing literature, the distribution of data is indicated as a normal distribution for the skewness and kurtosis in ranges of [−1, 1] and [−2, 2], respectively [115–117]. Thus, it can be concluded from Table 4 that the values of data sets are close to normal. The correlation matrix between the predictive variable and target (SHC) was shown in Fig. 4, which explains the linear correlation between all the variables. The Pearson correlation (P_c) between model inputs and target variables clearly demonstrated that the SHC of base fluid (P_c =0.8) has the highest linearity with the SHC of nanofluids among all the inputs and the remaining ones have similar Pearson correlation. To enhance the convergence acceleration of provided AI models, the predictive variables and targets are normalized into a range of [0, 1]. All the input-output datasets are normalized by the following formula:

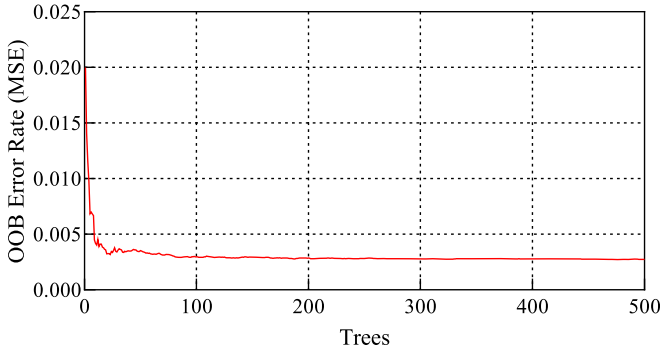

Fig. 6. The out-of-bag (OOB) MSE error versus the number of the tree for the RF model.

$$x_{nor} = \frac{x - x_{min}}{x_{max} - x_{min}} \tag{35}$$

where x, x_{nor},x_{max}, and $x_{min}$are the original value, normalized value, maximum, and minimum of the original value, respectively.

5. Results and discussion

As mentioned in the literature, the SHC of nanofluids is one of the most significant thermophysical properties, which has a crucial role in solar energy applications [5]. In this research, a probabilistic non-parametric approach namely GPR, RF, and GRNN model, which are the robust machine learning approaches, were used to provide an accurate prediction of the SHC of nanofluids based on four predictors variables including solid volume fraction (ϕ), temperature (T), mean diameter of nanoparticle (D_p), and SHC of base fluid (C_P^{Base}).

One of the most important advantages of the GPR model over other machine learning methods is its ability to capture the uncertainty of the model directly. GPR directly gives a distribution for the prediction value, rather than just one value as the prediction. Also, the GPR model is flexible and easy to implement. GPR gives the ability to add prior knowledge and specification about the shape of the model by selecting different types of kernels [94]. In order to develop the GPR model, five covariance functions comprised of Matern32, Matern52, Squared exponential, Rational quadratic, and Ard exponential was employed. The results of using each of the covariance functions in the GPR model are shown in Table 5, which indicates the superiority of the Ard exponential function due to having the highest correlation (0.999998 and 0.99974) and lowest RMSE (0.001153 J/K.g and 0.015064 J/K.g) in both training and testing stages, respectively. Besides, the Fig. 5 illustrated the predicted SHC of nanofluids distribution obtained from the covariance functions in comparison to the measured data points in the violin plot pattern for both training and testing modes. The performance of the "Ard exponential" function was significantly superior to others in the prediction of the SHC of nanofluids. As mentioned earlier, the hyper-parameters of the covariance function θ (σ_l , σ_f) were optimized automatically using gradient-based algorithms.

For the development of the RF model, the predictor variable number (m_{try}) in a trial and error process is selected in the range of [1,5], which

Table 6
The performance metrics of the provided AI-based models for the prediction of the SHC of nanofluids.

	Statistical criteria	GRP	RF	GRNN
Training stage	R	0.999998	0.99934	0.99984
	RMSE	0.00115	0.02317	0.01115
	MAPE	0.0230	0.4038	0.1060
	RAE	0.001279	0.021453	0.0052
	SI	0.000369	0.007421	0.00357
	I_w	0.99999	0.99966	0.99992
	AVE Rank	1	3	2
Testing stage	R	0.99974	0.99761	0.99563
	RMSE	0.01506	0.04598	0.06085
	MAPE	0.3092	1.0646	1.1237
	RAE	0.01476	0.0501	0.05266
	SI	0.00491	0.01497	0.01981
	I_w	0.99986	0.99871	0.99774
	AVE Rank	1	2	3

for a specific number of trees and based on the mean decrease in accuracy of prediction, was optimized to 4. At the first attempt for developing the RF model, the number of the trees was set equal to 1000, and the out-of-bag (OOB) error rate values were surveyed. The results demonstrated that the MSE value after 200 trees remained nearly unchanged, and the value of error equal to 0.27% (see Fig. 6), which implies that the convergence criterion is satisfied. Thus, m_{try} and n_{tree}were obtained 4 and 200, respectively.

It is worth noting that, for the GRNN model development, the neurons number and spread parameter are the critical setting factors, which in a trial and error procedure were selected as 0.005 and 100, respectively. In this study, the performance of the under-studied AI methods was evaluated using strong statistical criteria with the statistical results of the AI techniques in the training and testing stages, as listed in Table 6. Comparison of the results reflected in Table 6 demonstrated that the GPR model has the highest correlation with measured data sets values and the least error in the training stage (R=0.999998,

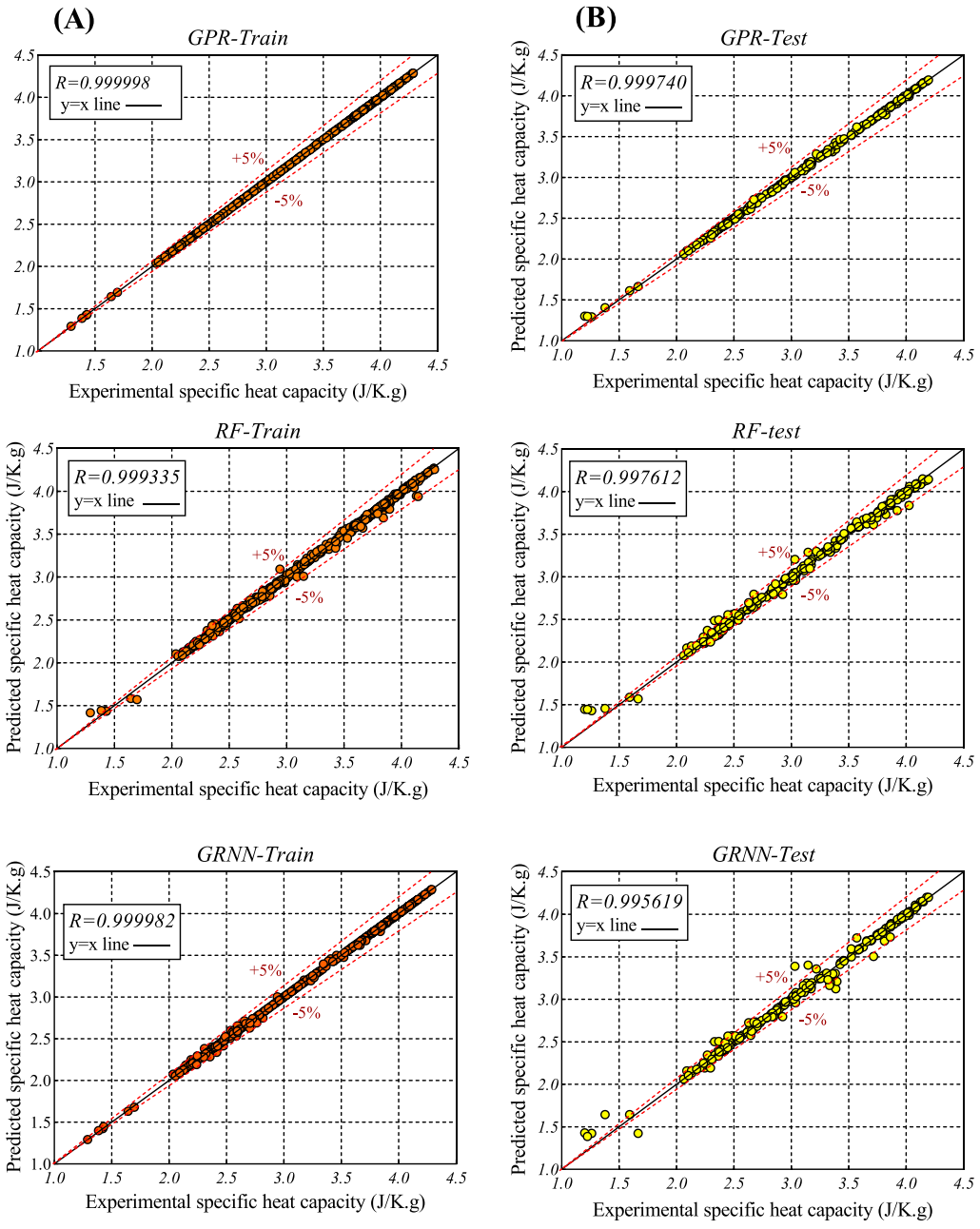

Fig. 7. The scatter plots of three predictive models for training (A) and testing (B) stages.

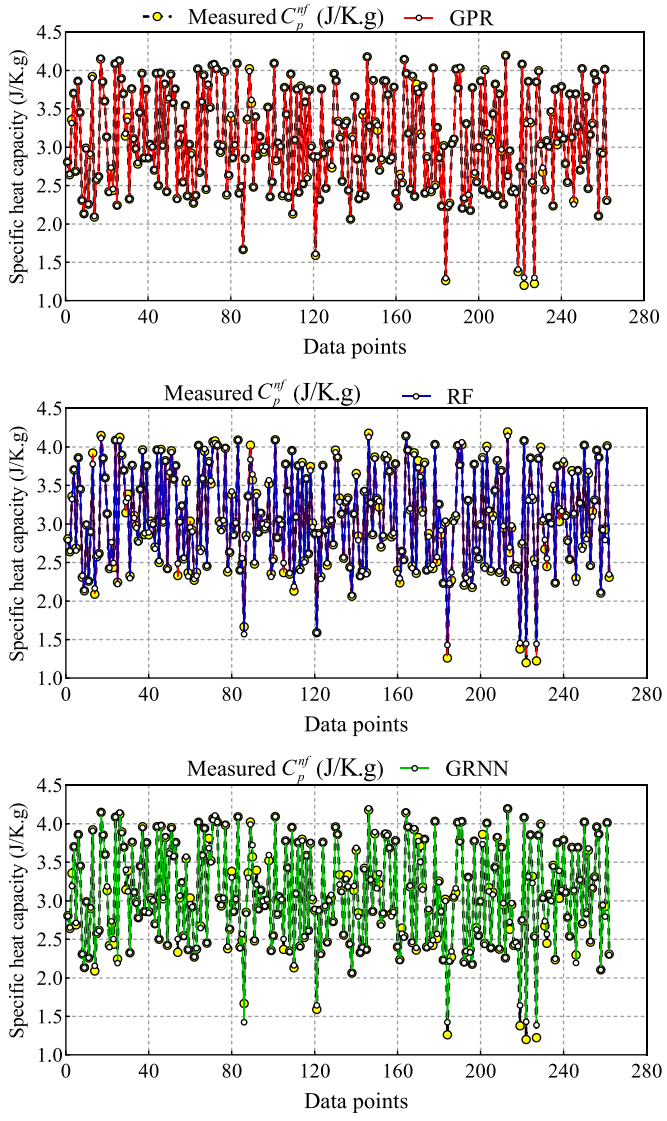

Fig. 8. The comparison between measured and predicted SHC of nanofluids values by three developed models in testing mode.

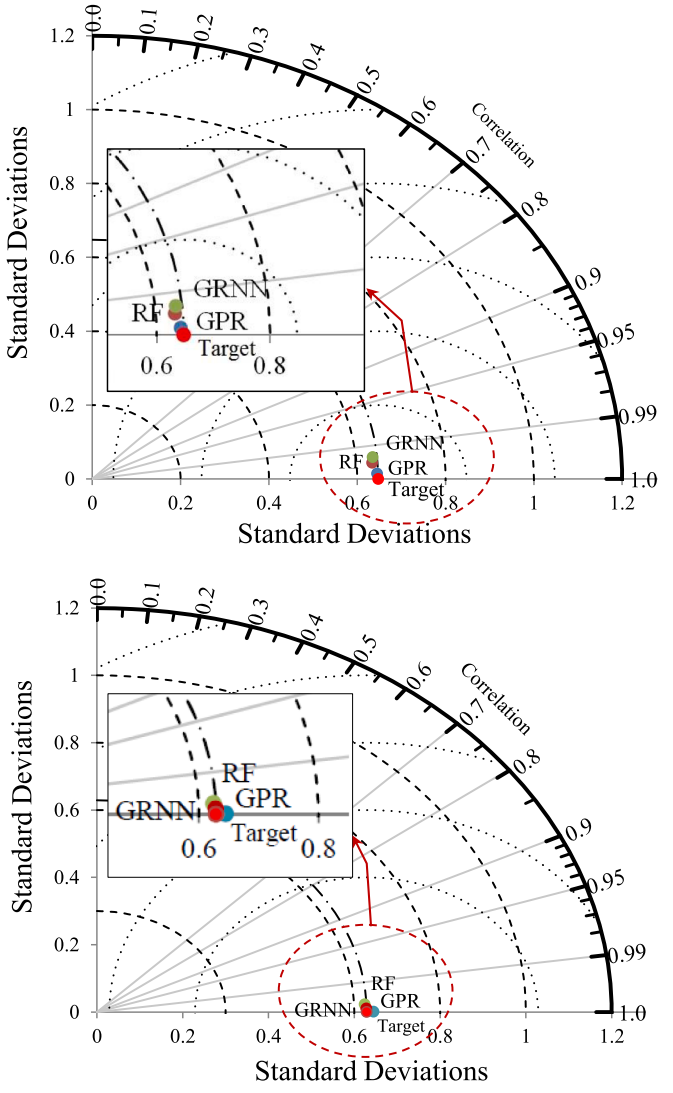

Fig. 9. Validation of the predictive performance of models in the training and testing stage using the Taylor diagrams.

RMSE=0.00115 J/K.g, MAPE=0.0230%, and I_w=0.99999) and testing stage (R=0.99974, RMSE=0.01506 J/K.g, MAPE=0.3092%, and I_w=0.99986), thereby making it the most superior model for estimating the SHC of nanofluid over RF and GRNN models. Moreover, the results showed the RF (R=0.99761, RMSE=0.04598 J/K.g) and GRNN (R=0.99563, RMSE=0.06085 J/K.g) models, as the second and third best ranks in the testing phase with good accuracy for assessing SHC of nanofluids.

Fig. 7 illustrates the scatter plots of three predictive models for the training (A) and testing (B) stages, which graphically and quantitatively describe the consistency of predicted and corresponding measured SHC values of nanofluids. It is crystal clear that the SHC of nanofluids (C_p^{nf}) values given by the GPR approach has the best fit with experimental data points than those obtained with RF and GRNN models. It must be noted that the best performance for the RF and GRNN is in the range of $C_p^{nf} \geq 2$ and $2 \leq C_p^{nf} \leq 3.25$, respectively. To better appreciate the performance of the predictive methods, Fig. 8 presents the predicted values and observations separately. It shows that the results of the GPR method are absolutely superior to the other ML-based models.

Taylor diagrams in the training and testing of three data-driven models are depicted in Fig. 9 for simultaneous evaluation of R, cRMSE, and standard deviation. A cursory glance at the location of the representation of each data-driven model relative to the target point indicates that there is a similar performance in the evaluation of C_p^{nf} values. However, by further magnifying the representation points, it can be seen that the ensemble method outperforms two other models in both training and testing phases due to the least physical distance from the target (red) point.

Error analysis was comprehensively conducted to efficiently assess the accuracy of developed models using Relative Deviation (RD) versus cumulative absolute error estimation. Fig. 10 depicted the relevant distribution of the relative deviation ($D_r = \frac{\mu_{r_o} - \mu_{r_i}}{\mu_{r_o}} \times 100$) for the three predictive models in the form of the violin (A) and diffusion plot (B) in both training and testing phases. According to Fig. 10, the error distribution of the GPR model has much more compression in the training phase than the RF and GRNN in both training and testing stages. Despite having a higher deviation range, the GRNN model was distributed in less compression in the testing phase than the RF. Furthermore, examining the relative deviation range of each method showed that the GPR model has the least range of deviation ($-8.4\% \leq E_r \leq 1.83\%$), and it, therefore, outperformed the RF ($-20.50\% \leq E_r \leq 7.50\%$) and GRNN ($-19.3\% \leq E_r \leq 14.6\%$) models.

Another error analysis was conducted on the expert validation of the

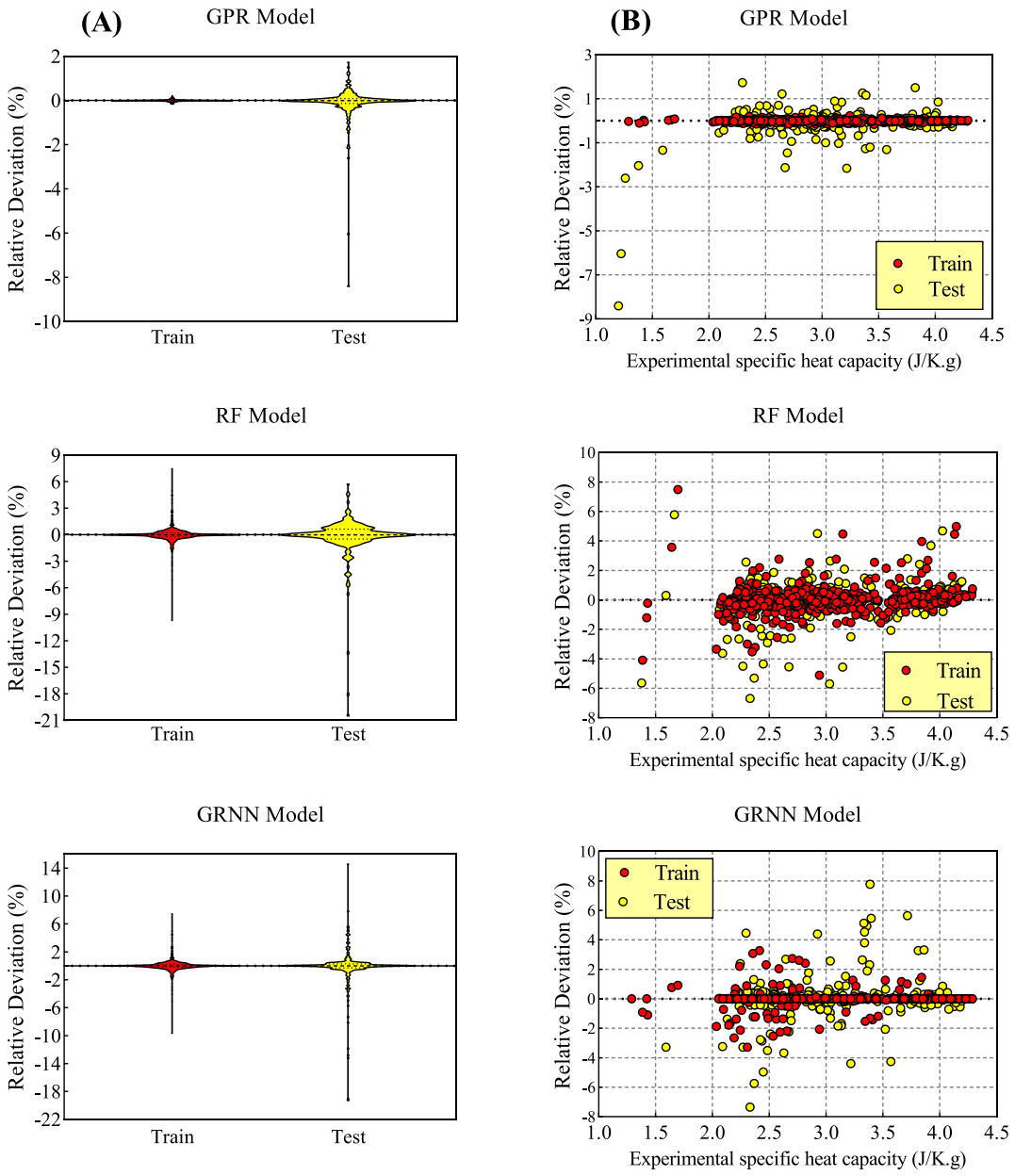

Fig. 10. The error distribution of the AI models in the form of the violin plot (A) and data point plot (B).

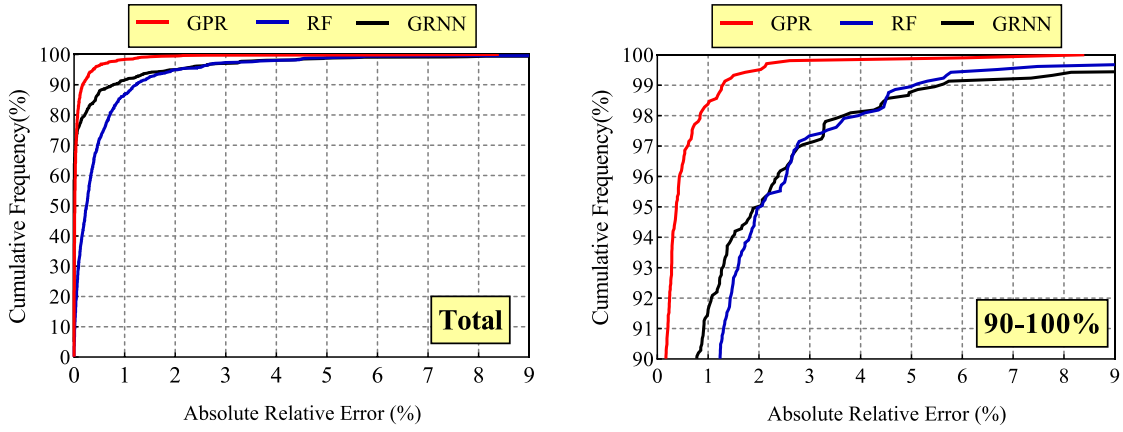

Fig. 11. The cumulative frequency versus the absolute relative error for all the models in the total frequency range (Left) and the range of (90 to 100%) (Right).

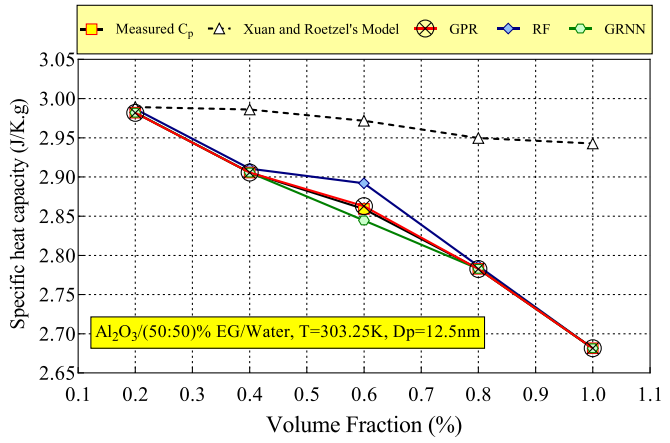

Fig. 12. Comparing the predicted SHC using AI-based models, Xuan and Roetzel's Model and experimental datasets for the nanofluids consist of Al_2O_3 by $T = 303.25K$in a mixture of 50:50% ethylene glycol (EG) and water (W) [57].

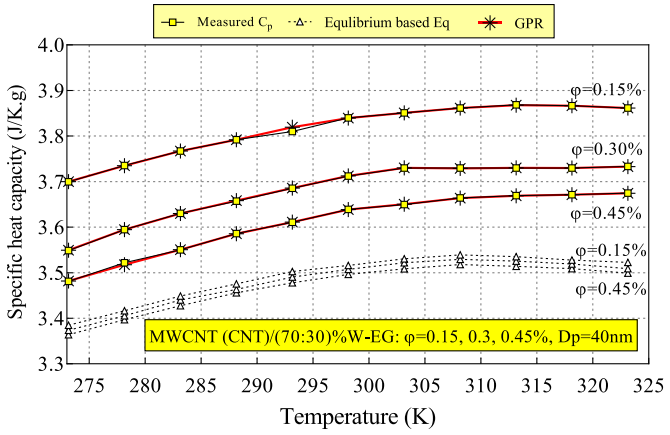

Fig. 13. Comparing the predicted SHC using the GPR model, equilibrium based Eq and experimental datasets for thee nanofluids consist of MWCNT by $\phi = 0.15, 0.3, 0.45\%$in a mixture of 30:70% ethylene glycol (EG) and water (W) [111].

AI-based model as a better computational model for estimating the SHC of nanofluids shows the percentage of cumulative versus the absolute percentage of relative error. Fig. 11 (Left) proves that more than 90 % of the predicted C_p^{nf} obtained from the GPR model has an absolute relative error of less than 0.17 % whereas the RF and GRNN have an absolute relative error of 1.23 % and 0.77 %, respectively. To examine more accurately the performance of the RF and GRNN models, the range of cumulative frequency in the range of 90 to 100 was magnified in Fig. 11 (Right) and observed that more than 95 % of the data have an error of less than 2 %. It can be concluded that the GRNN, developed by all the datasets, performs more efficiently than the RF technique. Regarding the results of error analysis, it can be deduced that the GRNN performs relatively better for the assessment of the SHC of nanofluids than the RF model despite having less correlation in the testing phase (R=0.99563) and higher error metrics (RMSE= 0.06085 J/K.g and MAPE=1.1237%).

Eventually, a physical trend of the SHC for four nanofluids was examined to better find the capabilities of the main AI model, and the results of consistency between experimental observations and AI models were compared with the aforementioned existing empirical correlations. Fig. 12 depicted the variation of the SHC a nanofluid including Al_2O_3 in a mixture of 50:50% ethylene glycol (EG) and water (W) [57] versus the volume fraction (%) obtained from three AI-based models, experimental

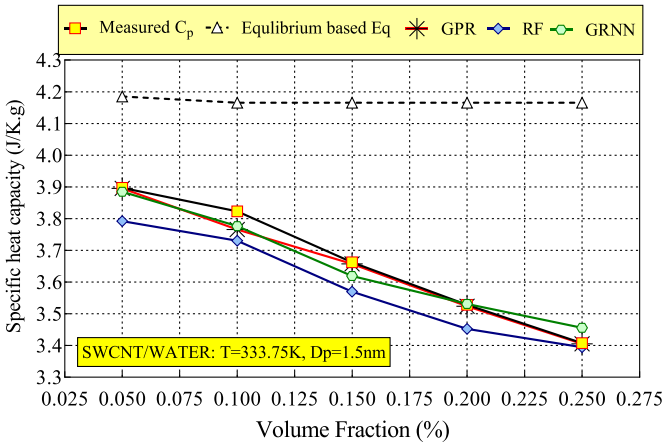

Fig. 14. Comparing the predicted SHC using three AI models, equilibrium based Eq and experimental datasets for nanofluids consist of SWCNT in water [61].

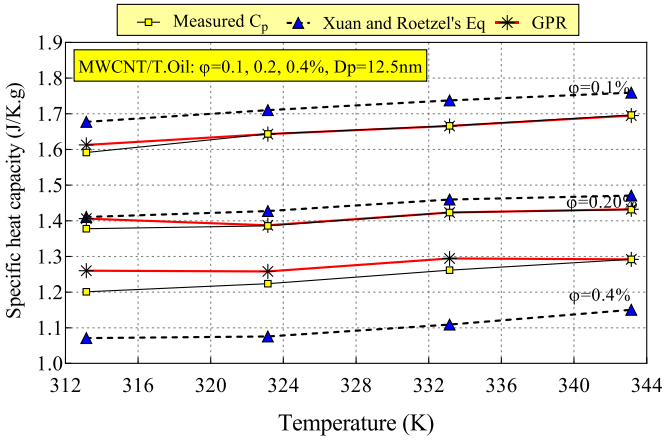

Fig. 15. Comparing the predicted SHC GPR model, Xuan and Roetzel's Model, and experimental datasets for thee nanofluids consist of MWCNT by $\phi = 0.1, 0.2, 0.4\%$in transfer oil [113].

data points, and Xuan and Roetzel's Model [118]. As seen in Fig. 12, the results indicated that SHC values predicted by the proposed GPR model results were in good agreement with the measured data points.

According to Fig. 13, the physical trend of the SHC of three nanofluids consists of MWCNT by φ= 0.15, 0.3, and 0.45 % in a mixture of 30:70 % ethylene glycol (EG) and water (W) [111] versus temperature (K) were conceptually depicted by using the GPR model and Eq. (4). From Fig. 13, it can be said that the ensemble model was successful in capturing the pattern of corresponding measured data points. In the next validation case, the variation of SWCNT in water versus the volume fraction [61] was illustrated for the purpose of the performance measurement of the AI models and Eq. (4), as shown in Fig. 14. The GPR model can optimally obtain the expected physical trend of the

Table 7
The sensitivity analysis of the model via the GPR model.

	All-φ	All-T	All-C_p^{Base}	All-D_p	All
R	0.96506	0.99913	0.88964	0.86752	0.99974
RMSE	0.16958	0.02708	0.29579	0.32198	0.01506
MAPE	4.77745	0.43474	5.14572	6.67815	0.30924
RAE	0.25811	0.02286	0.27069	0.38663	0.01476
SI	0.05522	0.00882	0.09631	0.10484	0.00490
I_W	0.98169	0.99956	0.93910	0.92333	0.99986
St.Dev	0.61828	0.64481	0.57021	0.54739	0.64481

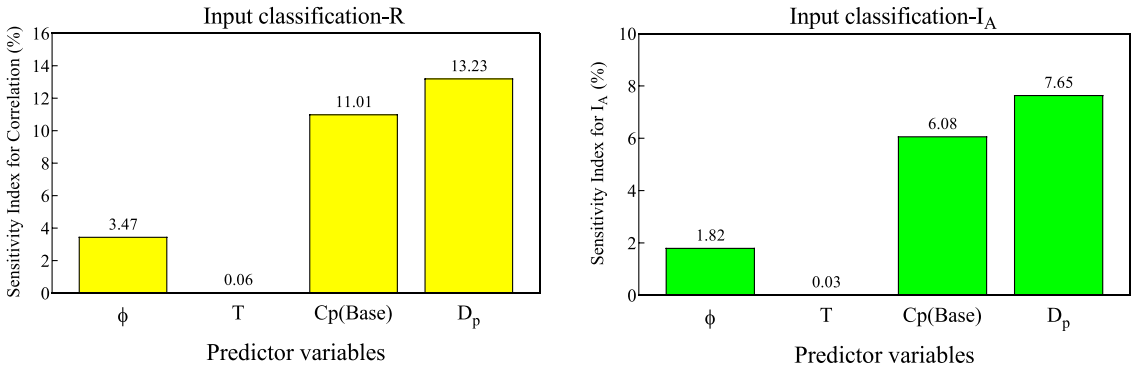

Fig. 16. Classification of predictive variables using sensitivity index for the prediction of nanofluids SHC on (Left) R and (Right) I_A.

corresponding measured datasets, followed by the GRNN and RF. In the last trend analysis case, Fig. 15 addresses the reliability and efficiency of the GPR in estimating the SHC of three types of nanofluids including MWCNT by φ=0.1, 0.2, and 0.4 % in transfer oil [113] in comparison with the Xuan and Roetzel's Model [118]. Obviously, the thermo-physical aspects of the validation cases express that the SHC of nanofluids values enhanced by increasing the temperature, whereas this trend will be reversed if the volume fraction is decreased.

6. Limitations and future research

The current work is focused on metal oxide and carbon material-based nanofluids in water, EG, and a mixture of them, which have many applications in the solar energy system. Recently, the new types of nanofluids comprised of metal oxide dispersed in the molten salt and their eutectics, such as alkali nitrate, alkali carbonate, or alkali-chlorides, widely considered in energy system applications. Those types of nanofluids are capable surprisingly to enhance the thermo-physical properties (i.e., specific heat capacity and thermal diffusivity) of base fluids. They have highly nonlinear behavior and can be considered as an evaluation of AI-based investigation in several aspects of energy storage systems. The ensemble stacking method can be a suitable AI-based selection for modeling the nonlinear behavior of thermal properties of the mentioned nanofluids, which can combine the advantages of several standalone AI approaches in a single model.

7. Sensitivity analysis

Sensitivity analysis in a predictive model demonstrates the degree of importance of predictive variables on the target. The dependence of the ϕ, T, D_p, and C_P^{Base}on the estimated SHC of nanofluid (C_P^{nf}) is examined, and it shows that the SHC of base fluid is considered to be the most crucial parameter due to its higher Pearson coefficient (r_p=0.8) as compared to the others. However, nonlinear relationships between input parameters and the target require that the importance of each one be assessed by subsequently excluding them using equalization to zero and preserving the rest of input variables in the predictive model [75,90,119]. For this purpose, the GPR model, as the best predictive AI model, was examined to survey the response of SHC based upon the degree of influence of each inputs using the statistical criteria (i.e., R, RMSE, MAPE, RAE, SI, I_w, and St.Dev).

According to Table 7, it can be concluded that the mean diameter of nanoparticle with the lowest correlation coefficient and agreement index (R=0.86752 and I_w=0.92333) and having the most error metrics (RMSE=0.32198 J/K.g, MAPE=6.67815% and RAE=0.38663) is known as the most sensitive parameter in estimating the SHC of nanofluids, followed by the SHC of the base fluid (R=0.88964 and RMSE=0.29579 J/K.g) and solid volume fraction (R= 0.96506 and RMSE=0.16958 J/K.g) in the next ranks. The sensitivity scaled indices are used to better show the effect of the input parameters (i.e.,ϕ, T, D_p, C_p^{Base}) using R and I_w in testing mode. Regrading to Fig. 16, it can be concluded that the mean diameter of nanoparticles (13.23% and 7.65%) and the SHC of the base fluid (11.01% and 6.08 %) with the highest sensitivity indices for R and I_w are the most effective factors in estimating the SHC of nanofluids, respectively.

8. Concluding remarks

In this study, we examined the application of ML algorithms in the prediction of the SHC of nanofluids using the GPR technique in comparison to the RF approach and GRNN. The models developed in this study used solid fraction volume (ϕ), temperature (T), mean diameter of nanoparticle (D_p), and the SHC of base fluid (C_P^{Base}) as model inputs. The models successfully predicted the SHC of nanofluids with a high degree of accuracy, showing that it is a viable alternative in the estimation of the specific heat capacity of the nanofluids than the seemingly time-consuming, expensive, and cumbersome experimental procedures. The GPR model with the best predictive performance (R=0.99974, RMSE=0.01506 J/K.g) outperformed the RF (R=0.99761, RMSE=0.04598 J/K.g), GRNN (R=0.99563, RMSE=0.06085 J/K.g), and existing convectional correlations in SHC assessment of nanofluids for solar energy applications. A proficient error analysis demonstrated that maximum absolute relative error of more than 90 % of the predicted data points for the GPR, RF, and GRNN models were 0.17 %, 1.23 %, and 0.77 %, respectively, which indicates the successful performance of all three AI methods in the meticulous estimation of SHC of nanofluids. Besides, the mean diameter of nanoparticles and the SHC of the base fluid by the highest sensitivity indices for R (13.23 % and 11.01 %) and I_w (7.65 % and 6.08 %) are the most influence in prediction of the SHC of nanofluids, respectively.

CRediT authorship contribution statement

Mehdi Jamei: Conceptualization, Methodology, Formal analysis, Software, Validation, Visualization, Writing - original draft. **Iman Ahmadianfar:** Methodology, Writing - original draft. **Ismail Adewale Olumegbon:** Methodology, Writing - original draft. **Masoud Karbasi:** Writing - original draft, Methodology, Writing - review & editing. **Amin Asadi:** Supervision, Writing - review & editing.

Declaration of Competing Interest

The authors declare that they have no known competing financial interests or personal relationships that could have appeared to influence the work reported in this paper.

References

[1] A. Naddaf, S. Zeinali Heris, Density and rheological properties of different nanofluids based on diesel oil at different mass concentrations: an experimental study, J. Therm. Anal. Calorim. 135 (2) (2019) 1229–1242.

[2] H. O'Hanley, J. Buongiorno, T. McKrell, L.-W. Hu. Measurement and model correlation of specific heat capacity of water-based nanofluids with silica, alumina and copper oxide nanoparticles. ASME International Mechanical Engineering Congress and Exposition 2011. pp. 1209-14.

[3] S.K. Das, S.U.S. Choi, A Review of Heat Transfer in Nanofluids, Adv. Heat Transf. 41 (2009) 81–197.

[4] I.M. Alarifi, H.M. Nguyen, A. Naderi Bakhtiyari, A. Asadi, Feasibility of ANFIS-PSO and ANFIS-GA models in predicting thermophysical properties of Al_2O_3-MWCNT/oil hybrid nanofluid, Materials 12 (21) (2019) 3628.

[5] J.R. Satti, D.K. Das, D. Ray, Specific heat measurements of five different propylene glycol based nanofluids and development of a new correlation, Int. J. Heat Mass Transf. 94 (2016) 343–353.

[6] I.M. Shahrul, I.M. Mahbubul, S.S. Khaleduzzaman, R. Saidur, M.F.M. Sabri, A comparative review on the specific heat of nanofluids for energy perspective, Renew. Sustain. Energy Rev. 38 (2014) 88–98. Elsevier Ltd.

[7] S.M.S. Murshed, C.A. Nieto de Castro, Conduction and convection heat transfer characteristics of ethylene glycol based nanofluids–a review, Appl. Energy (2016) 681–695. Elsevier Ltd.

[8] S. Soltani, A. Kasaeian, H. Sarrafha, D. Wen, An experimental investigation of a hybrid photovoltaic/thermoelectric system with nanofluid application, Sol. Energy 155 (2017) 1033–1043.

[9] J.J. Michael, S. Iniyan, Performance of copper oxide/water nanofluid in a flat plate solar water heater under natural and forced circulations, Energy Convers. Manage. 95 (2015) 160–169.

[10] U. Nithiyanantham, A. Zaki, Y. Grosu, L. González-Fernández, J.M. Igartua, A. Faik, SiO_2@ Al_2O_3 core-shell nanoparticles based molten salts nanofluids for thermal energy storage applications, J. Energy Storage 26 (2019), 101033.

[11] K. Farhana, K. Kadirgama, M.M. Rahman, D. Ramasamy, M.M. Noor, G. Najafi, et al., Improvement in the performance of solar collectors with nanofluids–a state-of-the-art review, Nano Struct. Nano Object 18 (2019), 100276. Elsevier B.V.

[12] Z. Wang, J. Qu, R. Zhang, X. Han, J. Wu, Photo-thermal performance evaluation on MWCNTs-dispersed microencapsulated PCM slurries for direct absorption solar collectors, J. Energy Storage 26 (2019), 100793.

[13] F.A. Boyaghchi, M. Chavoshi, V. Sabeti, Optimization of a novel combined cooling, heating and power cycle driven by geothermal and solar energies using the water/CuO (copper oxide) nanofluid, Energy 91 (2015) 685–699.

[14] A. Asadi, A.N. Bakhtiyari, I.M. Alarifi, Predictability evaluation of support vector regression methods for thermophysical properties, heat transfer performance, and pumping power estimation of MWCNT/ZnO–engine oil hybrid nanofluid, Eng. Comput. (2020).

[15] M. Hashemi-Tilehnoee, A. Dogonchi, S.M. Seyyedi, M. Sharifpur, Magneto-fluid dynamic and second law analysis in a hot porous cavity filled by nanofluid and nano-encapsulated phase change material suspension with different layout of cooling channels, J. Energy Storage 31 (2020), 101720.

[16] T.P. Otanicar, P.E. Phelan, R.S. Prasher, G. Rosengarten, R.A. Taylor, Nanofluid-based direct absorption solar collector, J. Renew. Sustain. Energy 2 (3) (2010), 033102. -.

[17] M. Milanese, G. Colangelo, A. Cretì, M. Lomascolo, F. Iacobazzi, A. De Risi, Optical absorption measurements of oxide nanoparticles for application as nanofluid in direct absorption solar power systems–part I: water-based nanofluids behavior, Sol. Energy Mater. Sol. Cells 147 (2016) 315–320.

[18] X. Li, G. Zeng, X. Lei, The stability, optical properties and solar-thermal conversion performance of SiC-MWCNTs hybrid nanofluids for the direct absorption solar collector (DASC) application, Sol. Energy Mater. Sol. Cells 206 (2020), 110323.

[19] I. Mahbubul, A. Saadah, R. Saidur, M. Khairul, A. Kamyar, Thermal performance analysis of Al_2O_3/R-134a nanorefrigerant, Int. J. Heat Mass Transf. 85 (2015) 1034–1040.

[20] S. Choudhary, A. Sachdeva, P. Kumar, Investigation of the stability of MgO nanofluid and its effect on the thermal performance of flat plate solar collector, Renew. Energy 147 (2020) 1801–1814.

[21] M. Heyhat, F. Kowsary, A. Rashidi, M. Momenpour, A. Amrollahi, Experimental investigation of laminar convective heat transfer and pressure drop of water-based Al_2O_3 nanofluids in fully developed flow regime, Exp. Therm. Fluid Sci. 44 (2013) 483–489.

[22] O. Mahian, L. Kolsi, M. Amani, P. Estellé, G. Ahmadi, C. Kleinstreuer, et al., Recent advances in modeling and simulation of nanofluid flows-part I: fundamentals and theory, Phys. Rep. 790 (2019) 1–48.

[23] K.S. Suganthi, K.S. Rajan, Metal oxide nanofluids: review of formulation, thermo-physical properties, mechanisms, and heat transfer performance, Renew. Sustain. Energy Rev. 76 (2017) 226–255. Elsevier Ltd.

[24] D. Cabaleiro, C. Gracia-Fernández, J.L. Legido, L. Lugo, Specific heat of metal oxide nanofluids at high concentrations for heat transfer, Int. J. Heat Mass Transf. 88 (2015) 872–879.

[25] K. Kwak, C. Kim, Viscosity and thermal conductivity of copper oxide nanofluid dispersed in ethylene glycol. 2005. p. 35-40.

[26] K.S. Suganthi, KS. Rajan, Temperature induced changes in ZnO-water nanofluid: zeta potential, size distribution and viscosity profiles, Int. J. Heat Mass Transf. 55 (25-26) (2012) 7969–7980.

[27] L. Lu, Z.H. Liu, H.S. Xiao, Thermal performance of an open thermosyphon using nanofluids for high-temperature evacuated tubular solar collectors. Part 1: indoor experiment, Sol. Energy 85 (2) (2011) 379–387.

[28] T. Yousefi, F. Veysi, E. Shojaeizadeh, S. Zinadini, An experimental investigation on the effect of Al_2O_3-H_2O nanofluid on the efficiency of flat-plate solar collectors, Renew. Energy 39 (1) (2012) 293–298.

[29] M. Mirzaei, Experimental investigation of the assessment of Al_2O_3-H_2O and CuO-H_2O nanofluids in a solar water heating system, J. Energy Storage 14 (2017) 71–81.

[30] M.A. Sabiha, R. Saidur, S. Hassani, Z. Said, S. Mekhilef, Energy performance of an evacuated tube solar collector using single walled carbon nanotubes nanofluids, Energy Convers. Manage. 105 (2015) 1377–1388.

[31] Y. Tong, J. Kim, H. Cho, Effects of thermal performance of enclosed-type evacuated U-tube solar collector with multi-walled carbon nanotube/water nanofluid, Renew. Energy 83 (2015) 463–473.

[32] S. Manikandan, K.S. Rajan, Sand-propylene glycol-water nanofluids for improved solar energy collection, Energy 113 (2016) 917–929.

[33] K.S. Suganthi, Vinodhan V. Leela, K.S. Rajan, ZnO–propylene glycol–water nanofluids with improved properties for potential applications in renewable energy and thermal management, Colloids Surf. A 506 (2016) 63–73.

[34] Q. He, S. Zeng, S. Wang, Experimental investigation on the efficiency of flat-plate solar collectors with nanofluids, Appl. Therm. Eng. 88 (2014) 165–171.

[35] A. Zamzamian, M. KeyanpourRad, M. KianiNeyestani, M.T. Jamal-Abad, An experimental study on the effect of Cu-synthesized/EG nanofluid on the efficiency of flat-plate solar collectors, Renew. Energy 71 (2014) 658–664.

[36] S. Akilu, A.T. Baheta, K.V. Sharma, M.A. Said, Experimental determination of nanofluid specific heat with SiO2 nanoparticles in different base fluids, in: Conference experimental determination of nanofluid specific heat with SiO2 nanoparticles in different base fluids, AIP Conference Proceedings, 1877, American Institute of Physics Inc, 2017, p. 090001. AIP Conference Proceedings.

[37] H.A. Al-Jamimi, T.A. Saleh, Transparent predictive modelling of catalytic hydrodesulfurization using an interval type-2 fuzzy logic, J. Clean. Prod. 231 (2019) 1079–1088.

[38] A. Mohebbi, Prediction of specific heat and thermal conductivity of nanofluids by a combined equilibrium and non-equilibrium molecular dynamics simulation, J. Mol. Liq. 175 (2012) 51–58.

[39] G. Sadeghi, S. Nazari, M. Ameri, F. Shama, Energy and exergy evaluation of the evacuated tube solar collector using Cu_2O/water nanofluid utilizing ANN methods, Sustain. Energy Technol. Assess. 37 (2020), 100578.

[40] H. Riazi, T. Murphy, G.B. Webber, R. Atkin, S.S.M. Tehrani, R.A. Taylor, Specific Heat Control of Nanofluids: a Critical Review, Elsevier Masson SAS, 2016, pp. 25–38.

[41] B. Barbés, R. Páramo, E. Blanco, M.J. Pastoriza-Gallego, M.M. Piñeiro, J. L. Legido, et al., Thermal conductivity and specific heat capacity measurements of Al_2O_3 nanofluids, J. Therm. Anal. Calorim. 111 (2) (2013) 1615–1625.

[42] G. Huminic, A. Huminic, Application of nanofluids in heat exchangers: a review, Renew. Sustain. Energy Rev. 16 (8) (2012) 5625–5638. Pergamon.

[43] B.C. Pak, Y.I. Cho, Hydrodynamic and heat transfer study of dispersed fluids with submicron metallic oxide particles, Exp. Heat Transf. Int. J. 11 (2) (1998) 151–170.

[44] Z. Liu, Q. Zhu, Application of aqueous nanofluids in a horizontal mesh heat pipe, Energy Convers. Manage. 52 (1) (2011) 292–300.

[45] J.A. Eastman, S. Choi, S. Li, W. Yu, L. Thompson, Anomalously increased effective thermal conductivities of ethylene glycol-based nanofluids containing copper nanoparticles, Appl. Phys. Lett. 78 (6) (2001) 718–720.

[46] T.-P. Teng, Y.-H. Hung, T.-C. Teng, J.-H. Chen, Performance evaluation on an air-cooled heat exchanger for alumina nanofluid under laminar flow, Nanoscale Res. Lett. 6 (1) (2011) 488.

[47] J.M. Smith, Introduction to chemical engineering thermodynamics, J. Chem. Educ. 27 (10) (1950) 584. -.

[48] J. Buongiorno, Convective transport in nanofluids, J. Heat Transf. 128 (3) (2006) 240–250.

[49] B. Barbés, R. Páramo, E. Blanco, C. Casanova, Thermal conductivity and specific heat capacity measurements of CuO nanofluids, J. Therm. Anal. Calorim. 115 (2) (2014) 1883–1891.

[50] I.O. Alade, M.A. Abd Rahman, A. Bagudu, Z. Abbas, Y. Yaakob, T.A. Saleh, Development of a predictive model for estimating the specific heat capacity of metallic oxides/ethylene glycol-based nanofluids using support vector regression, Heliyon 5 (6) (2019).

[51] H. Khodadadi, S. Aghakhani, H. Majd, R. Kalbasi, S. Wongwises, M. Afrand, A comprehensive review on rheological behavior of mono and hybrid nanofluids: effective parameters and predictive correlations, Int. J. Heat Mass Transf. Part B 127 (2018) 997–1012. Elsevier Ltd.

[52] M.A. Hassan, D. Banerjee, A soft computing approach for estimating the specific heat capacity of molten salt-based nano fluids, J. Mol. Liq. 281 (2019) 365–375.

[53] T.-P. Teng, Y.-H. Hung, Estimation and experimental study of the density and specific heat for alumina nanofluid, J. Exp. Nanosci. 9 (7) (2014) 707–718.

[54] Y.R. Sekhar, K. Sharma, Study of viscosity and specific heat capacity characteristics of water-based Al_2O_3 nanofluids at low particle concentrations, J. Exp. Nanosci. 10 (2) (2015) 86–102.

[55] R.S. Vajjha, D.K. Das, Specific heat measurement of three nanofluids and development of new correlations, J. Heat Transf. 131 (7) (2009) 071601.

[56] S.-Q. Zhou, R. Ni, Measurement of the specific heat capacity of water-based Al2O3 nanofluid measurement of the specific heat capacity of water-based Al2O3 nanofluid. 2012;093123(2008):1-4.

[57] M. Elias, I. Mahbubul, R. Saidur, M. Sohel, I. Shahrul, S. Khaleduzzaman, et al., Experimental investigation on the thermo-physical properties of Al_2O_3 nanoparticles suspended in car radiator coolant, Int. Commun. Heat Mass Transf. 54 (2014) 48–53.

[58] E.D. Robertis, E.H.H. Cosme, R.S. Neves, A.Y. Kuznetsov, A.P.C. Campos, S. M. Landi, et al., Application of the modulated temperature differential scanning calorimetry technique for the determination of the specific heat of copper nano fl uids, Appl. Therm. Eng. 41 (2012) 10–17.

[59] A.K. Starace, J.C. Gomez, J. Wang, S. Pradhan, G.C. Glatzmaier, A.K. Starace, et al. Nanofluid heat capacities nanofluid heat capacities. 2011;124323.

[60] V. Kumaresan, R. Velraj, Experimental investigation of the thermo-physical properties of water–ethylene glycol mixture based CNT nanofluids, Thermochim. Acta 545 (2012) 180–186.

[61] M. Sabiha, R. Mostafizur, R. Saidur, S. Mekhilef, Experimental investigation on thermo physical properties of single walled carbon nanotube nanofluids, Int. J. Heat Mass Transf. 93 (2016) 862–871.

[62] S.M.S. Murshed, Determination of effective specific heat of nanofluids, J. Exp. Nanosci. 6 (2011) 8080.

[63] H.-m. Nieh, T.-p. Teng, C.-c. Yu, Enhanced heat dissipation of a radiator using oxide nano-coolant, Int. J. Therm. Sci. 77 (2014) 252–261.

[64] X. Li, W. Chen, C. Zou, An experimental study on β -cyclodextrin modified carbon nanotubes nanofluids for the direct absorption solar collector (DASC): specific heat capacity and photo-thermal conversion performance, Sol. Energy Mater. Sol. Cells 204 (1) (2020), 110240. -.

[65] M. Jamei, R. Pourrajab, I. Ahmadianfar, A. Noghrehabadi, Accurate prediction of thermal conductivity of ethylene glycol-based hybrid nanofluids using artificial intelligence techniques, Int. Commun. Heat Mass Transf. 116 (2020), 104624.

[66] R. Pourrajab, I. Ahmadianfar, M. Jamei, M. Behbahani, A meticulous intelligent approach to predict thermal conductivity ratio of hybrid nanofluids for heat transfer applications, J. Therm. Anal. Calorim. (2020) 1–18.

[67] A. Asadi, I.M. Alarifi, H.M. Nguyen, H. Moayedi, Feasibility of least-square support vector machine in predicting the effects of shear rate on the rheological properties and pumping power of MWCNT–MgO/oil hybrid nanofluid based on experimental data, J. Therm. Anal. Calorim. (2020) 1–16.

[68] M. Liu, J. Severino, F. Bruno, P. Majewski, Experimental investigation of specific heat capacity improvement of a binary nitrate salt by addition of nanoparticles/microparticles, J. Energy Storage 22 (2019) 137–143.

[69] A. Pare, S.K. Ghosh, A unique thermal conductivity model (ANN) for nanofluid based on experimental study, Powder Technol. 377 (2021) 429–438.

[70] A. Naseri, M. Jamei, I. Ahamadianfar, M. Behebahani, Nanofluids thermal conductivity prediction applying a novel hybrid data-driven model validated using Monte Carlo based sensitivity analysis, Eng. Comput. (2020).

[71] A. Asadi, A. Naderi, B. Ibrahim, Predictability evaluation of support vector regression methods for thermophysical properties, heat transfer performance, and pumping power estimation of MWCNT/ZnO–engine oil hybrid nanofluid, Eng. Comput. (2020), 0123456789.

[72] M.H. Ahmadi, B. Mohseni-Gharyehsafa, M. Farzaneh-Gord, R.D. Jilte, R. Kumar, K.-w. Chau, Applicability of connectionist methods to predict dynamic viscosity of silver/water nanofluid by using ANN-MLP, MARS and MPR algorithms, Eng. Appl. Comput. Fluid Mech. 13 (1) (2019) 220–228.

[73] M.K. Meybodi, S. Naseri, A. Shokrollahi, A. Daryasafar, Prediction of viscosity of water-based Al_2O_3, TiO_2, SiO_2, and CuO nanofluids using a reliable approach, Chemom. Intell. Lab. Syst. 149 (2015) 60–69.

[74] F. Yousefi, H. Karimi, M.M. Papari, Modeling viscosity of nanofluids using diffusional neural networks, J. Mol. Liq. 175 (2012) 85–90.

[75] M. Jamei, I. Ahmadianfar, A rigorous model for prediction of viscosity of oil-based hybrid nanofluids, Phys. A 556 (2020), 124827.

[76] I.O. Alade, M.A.A. Rahman, T.A. Saleh, An approach to predict the isobaric specific heat capacity of nitrides/ethylene glycol-based nanofluids using support vector regression, J. Energy Storage 29 (February) (2020), 101313. -.

[77] I.O. Alade, M.A. Abd Rahman, T.A. Saleh, Modeling and prediction of the specific heat capacity of Al_2O_3/water nanofluids using hybrid genetic algorithm/support vector regression model, Nano-Struct. Nano-Objects 17 (2019) 103–111.

[78] I.O. Alade, M.A. Abd Rahman, T.A. Saleh, Predicting the specific heat capacity of alumina/ethylene glycol nanofluids using support vector regression model optimized with Bayesian algorithm, Sol. Energy 183 (2019) 74–82.

[79] G.A. Longo, C. Zilio, E. Ceseracciu, M. Reggiani, Application of artificial neural network (ANN) for the prediction of thermal conductivity of oxide-water nanofluids, Nano Energy 1 (2) (2012) 290–296.

[80] M.A. Ariana, B. Vaferi, G. Karimi, Prediction of thermal conductivity of alumina water-based nanofluids by artificial neural networks, Powder Technol. 278 (2015) 1–10.

[81] M.K. Meybodi, A. Daryasafar, M.M. Koochi, J. Moghadasi, R.B. Meybodi, A. K. Ghahfarokhi, A novel correlation approach for viscosity prediction of water based nanofluids of Al_2O_3, TiO_2, SiO_2 and CuO, J. Taiwan Inst. Chem. Eng. 58 (2016) 19–27.

[82] A. Hemmati-Sarapardeh, A. Varamesh, M.M. Husein, K. Karan, On the evaluation of the viscosity of nanofluid systems: modeling and data assessment, Renew. Sustain. Energy Rev. 81 (2018) 313–329.

[83] S. Khosrojerdi, M. Vakili, M. Yahyaei, K. Kalhor, Thermal conductivity modeling of graphene nanoplatelets/deionized water nanofluid by MLP neural network and theoretical modeling using experimental results, Int. Commun. Heat Mass Transf. 74 (2016) 11–17.

[84] I. Olanrewaju, M. Amiruddin, A. Rahman, Y. Yaakob, Application of support vector regression and artificial neural network for prediction of specific heat capacity of aqueous nano fluids of copper oxide. 2020;197(December 2019):485-90.

[85] I. Olanrewaju, M. Amiruddin, A. Rahman, A. Bagudu, Y. Yaakob, A. Saleh, Heliyon development of a predictive model for estimating the specific heat capacity of metallic oxides/ethylene glycol-based nano fl uids using support vector regression. 5(6) (2019).

[86] P.C. Mukesh Kumar, R. Kavitha, Regression analysis and behavioral study of predictor factors on thermal conductivity of nanofluids using soft computing tool, Mater. Today 21 (xxxx) (2020) 438–444.

[87] Y. Zhang, X. Xu, Predicting the thermal conductivity enhancement of nanofluids using computational intelligence, Phys. Lett. Sect. A 384 (20) (2020), 126500. -.

[88] K. Liu, Y. Li, X. Hu, M. Lucu, W.D. Widanage, Gaussian process regression with automatic relevance determination kernel for calendar aging prediction of lithium-ion batteries, IEEE Trans. Ind. Inf. 16 (6) (2019) 3767–3777.

[89] Z. Deng, X. Hu, X. Lin, Y. Che, L. Xu, W. Guo, Data-driven state of charge estimation for lithium-ion battery packs based on Gaussian process regression, Energy 205 (2020), 118000.

[90] M. Gholizadeh, M. Jamei, I. Ahmadianfar, R. Pourrajab, Prediction of nanofluids viscosity using random forest (RF) approach, Chemom. Intell. Lab. Syst. 201 (2020), 104010.

[91] M. Balcilar, A.S. Dalkilic, A. Suriyawong, T. Yiamsawas, S. Wongwises, Investigation of pool boiling of nanofluids using artificial neural networks and correlation development techniques, Int. Commun. Heat Mass Transf. 39 (3) (2012) 424–431.

[92] R. Grbić, D. Kurtagić, D. Slišković, Stream water temperature prediction based on Gaussian process regression, Expert Syst. Appl. 40 (18) (2013) 7407–7414.

[93] C.K. Williams, C.E. Rasmussen, Gaussian proCesses for Machine Learning, MIT Press, Cambridge, MA, 2006.

[94] C.E. Rasmussen, CK. Williams, Gaussian Processes for Machine Learning, 38, The MIT Press, Cambridge, MA, USA, 2006, pp. 715–719, 2006.

[95] D.F. Specht, A general regression neural network, IEEE Trans. Neural Netw. 2 (6) (1991) 568–576.

[96] Ö. Polat, T. Yildirim, Genetic optimization of GRNN for pattern recognition without feature extraction, Expert Syst. Appl. 34 (4) (2008) 2444–2448.

[97] L. Breiman, Random forests, Mach. Learn. 45 (1) (2001) 5–32.

[98] T.K. Ho, Random decision forests. Proceedings of 3rd international conference on document analysis and recognition. IEEE1995. pp. 278-82.

[99] P. Vorpahl, H. Elsenbeer, M. Märker, B. Schröder, How can statistical models help to determine driving factors of landslides? Ecol. Model. 239 (2012) 27–39.

[100] H.R. Pourghasemi, N. Kerle, Random forests and evidential belief function-based landslide susceptibility assessment in Western Mazandaran Province, Iran, Environ. Earth Sci. 75 (3) (2016) 185.

[101] K.K. Nicodemus, J.D. Malley, Predictor correlation impacts machine learning algorithms: implications for genomic studies, Bioinformatics 25 (15) (2009) 1884–1890.

[102] O. Rahmati, H.R. Pourghasemi, A.M. Melesse, Application of GIS-based data driven random forest and maximum entropy models for groundwater potential mapping: a case study at Mehran Region, Iran, CATENA 137 (2016) 360–372.

[103] K. Taalab, T. Cheng, Y. Zhang, Mapping landslide susceptibility and types using random forest, Big Earth Data 2 (2) (2018) 159–178.

[104] A. Liaw, M. Wiener, Classification and regression by randomForest, R News 2 (3) (2002) 18–22.

[105] C.J. Willmott, Some comments on the evaluation of model performance, Bull. Am. Meteorol. Soc. 63 (11) (1982) 1309–1313.

[106] C.D. Lewis, Industrial and Business Forecasting Methods: a Practical Guide to Exponential Smoothing and Curve Fitting, Butterworth-Heinemann, 1982.

[107] K.E. Taylor, Summarizing multiple aspects of model performance in a single diagram, J. Geophys. Res 106 (D7) (2001) 7183–7192.

[108] I. Ahmadianfar, M. Jamei, X. Chu, Prediction of local scour around circular piles under waves using a novel artificial intelligence approach, Mar. Georesour. Geotechnol. (2019) 1–12.

[109] M. Jamei, I. Ahmadianfar, Prediction of scour depth at piers with debris accumulation effects using linear genetic programming, Mar. Georesour. Geotechnol. 38 (2020) 468–479.

[110] B. Barbés, R. Páramo, E. Blanco, M.J. Pastoriza-Gallego, M.M. Pineiro, J.L. Legido, et al., Thermal conductivity and specific heat capacity measurements of Al_2O_3 nanofluids, J. Therm. Anal. Calorim. 111 (2) (2013) 1615–1625.

[111] V. Kumaresan, R. Velraj, Experimental investigation of the thermo-physical properties of water–ethylene glycol mixture based CNT nanofluids, Thermochim. Acta 545 (2012) 180–186.

[112] Q. He, S. Wang, M. Tong, Y. Liu, Experimental study on thermophysical properties of nanofluids as phase-change material (PCM) in low temperature cool storage, Energy Convers. Manage. 64 (2012) 199–205.

[113] M.F. Pakdaman, M. Akhavan-Behabadi, P. Razi, An experimental investigation on thermo-physical properties and overall performance of MWCNT/heat transfer oil nanofluid flow inside vertical helically coiled tubes, Exp. Therm. Fluid Sci. 40 (2012) 103–111.

[114] X. Li, W. Chen, C. Zou, An experimental study on β-cyclodextrin modified carbon nanotubes nanofluids for the direct absorption solar collector (DASC): specific heat capacity and photo-thermal conversion performance, Sol. Energy Mater. Sol. Cells 204 (2020), 110240.

[115] F.J. Gravetter, L.B. Wallnau, L.-A.B. Forzano, J.E. Witnauer, Essentials of Statistics for the Behavioral Sciences, Cengage Learning, 2020.

[116] A. Desgagné, P. Lafaye de Micheaux, A powerful and interpretable alternative to the Jarque–Bera test of normality based on 2nd-power skewness and kurtosis,

using the Rao's score test on the APD family, J. Appl. Statist. 45 (13) (2018) 2307–2327.
[117] F. Andy, Discovering Statistics Using SPSS for Windows: Advanced Techniques for the Beginner, Sage Publications, 2000.
[118] Y. Xuan, W. Roetzel, Conceptions for heat transfer correlation of nanofluids, Int. J. Heat Mass Transf. 43 (19) (2000) 3701–3707.
[119] P. Burman, A comparative study of ordinary cross-validation, v-fold cross-validation and the repeated learning-testing methods, Biometrika 76 (3) (1989) 503–514.